Biomass-derived carbon electrodes for supercapacitors and hybrid solar cells: towards sustainable photo-supercapacitors

Nilanka M Keppetipola, Céline Olivier, Thierry Toupance, Ludmila Cojocaru

Biomass-derived carbon electrodes for supercapacitors and hybrid solar cells: towards sustainable photo-supercapacitors

Nilanka M. Keppetipola, Céline Olivier, Thierry Toupance, and Ludmila Cojocaru**

Institut des Sciences Moléculaires, UMR 5255 CNRS, Université de Bordeaux, 351 Cours de la Libération, F-33405 Talence Cedex, France

KEYWORDS: biomass-derived carbon electrodes, carbon-supercapacitor, carbon-hybrid solar cells, photo-supercapacitors, solar-energy conversion-storage devices.

ABSTRACT: Due to their outstanding electrochemical properties, electrical conductivity, flexibility, and low-cost, carbon materials open up new opportunities for the design of compact devices with a wide variety of potential applications. Biomass renewable resources for carbon material preparation have attracted huge attention in the last years due to widespread availability, low-cost processing and high-performance of the resulting porous carbons for sustainable technologies applications. For example, the porosity and morphology of carbon materials, which can be tuned by different activation methods, govern the ion diffusion rate during the supercapacitors charge/discharge processes. On the other hand, carbon electrodes have been applied as electrodes for dye-sensitized and perovskite solar cells, thanks to their low fabrication cost, compact structure, and optimized interfaces which play a key role in charge collection and stability of the devices. Moreover, due to the possibility of using carbon electrodes for storage and conversion devices, efficient methods to harvest and store energy in one single device are crucial for technology advancement and the energy transition process. This contribution aims to review the advances made in the use of carbon-materials obtained from biomass sources as electrodes for storage and energy conversion devices, and the future application of shared and/or distinct carbon electrodes for the development of integrated power packs including supercapacitors and dye-sensitized or perovskite solar cells. The storage properties of supercapacitors are discussed in terms of textural characteristics of biomass-derived activated carbons while the photovoltaic parameters of solar cells based of bio-sourced carbons are compared with those of devices using conventional metal-based electrodes. Finally, a specific emphasis concerns on the energy conversion-storage efficiencies of solar cell-supercapacitor integrated devices.

1. INTRODUCTION

Driven by the ever-ongoing energy demand growth, the development of high-performance, low-cost, and clean energy technologies is an urgent need in order to reduce the use of fossil fuels and environmental pollution. Among all energy-related technologies, energy storage and energy conversion devices such as supercapacitors (SCs), dye-sensitized solar cells (DSCs) or perovskite solar cells (PSCs) have been extensively investigated.[1-3] However, the materials used for the design of efficient and low-cost devices play a crucial role.[4-6] Carbon materials have opened up new opportunities and have been successfully applied for a wide variety of purposes. Most of the carbon materials employed in energy conversion devices are derived from non-renewable resources such as fossil-fuels. In this regard the use of biomass, that is widely available in nature, allows the implementation of carbon materials in sustainable technologies applications such as SCs, DSCs and PSCs which is still a topic under development. Thus, several benchmark reviews have discussed the use of conventional or biomass-derived carbon materials for supercapacitor and for photovoltaic applications. [7-11]

For solar cells technologies, intermittency constitutes one major limitation for substituting conventional fossil fuels energy resources. High photovoltaic energy conversion efficiencies are indeed reached when the sun directly illuminates the solar panels, albeit only a few hours per day. In this context, pack-devices containing solar cells and storage devices, called photo-batteries[12-14] or photo-SCs,[15-18] have been developed as solution for device with continuous power generation. Due to the fact that carbon can be used as electrode material for both supercapacitors and hybrid solar cells, the devices can be connected through a carbon bridge electrode as shown in Figure 1a. Such devices, composed of carbon-based solar cell and carbon-based storage device in one single pack, can simultaneously harvest and store energy from the sunlight to satisfy the requirements of

some application fields requiring specific properties such as small size, lightweight, and high energy density. A brief literature overview revealed that solely eighteen papers related to the integrated hybrid solar cells with supercapacitors have been published so far, of which twelve are describing DSC/SC and six the PSC/SC systems (Figure 1.b).

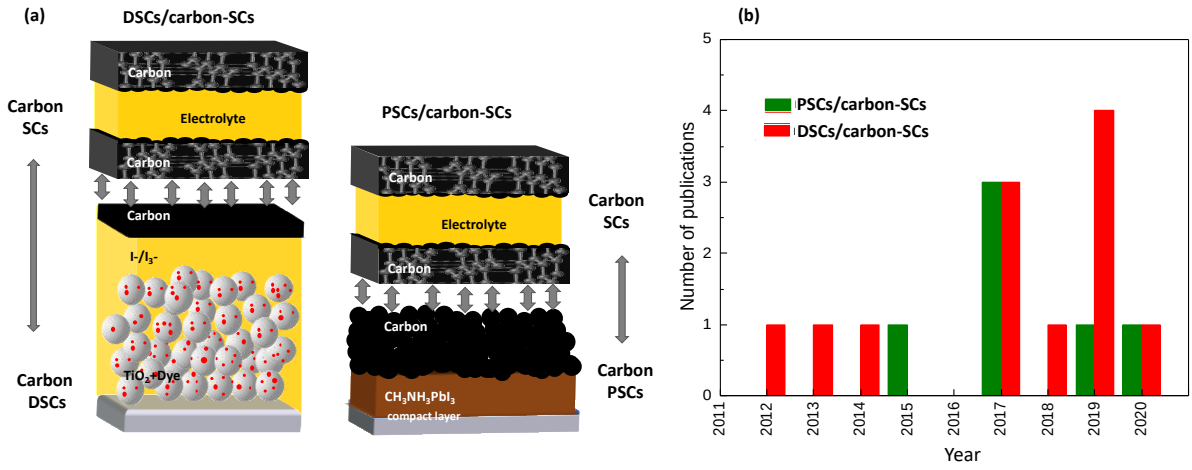

Figure 1. (a) Architecture of integrated devices including hybrid solar cells and supercapacitor sharing a common carbon electrode; (b) the number of publications using "carbon integrated dye-sensitized solar cells/supercapacitors, DSCs/carbon-SCs" and "carbon integrated perovskite solar cells/supercapacitors, PSCs/carbon-SCs" keywords surveyed in Scopus database.

To the best of our knowledge, no effort has been devoted on the application of biomass-based activated carbon (AC) in integrated energy conversion-storage systems that could be interesting for future application as sustainable compact electronics. Up to now the best performing carbon-based DSCs-SCs integrated device, showing an overall efficiency of 5.12%, was obtained by using an ethylene-derived multiwalled carbon nanotubes (MWCNTs) electrode[15] while values over 10%

were reported for a carbon-based PSCs-SCs power pack using carbon composite (MWCNTs/pyrrole/bacterial cellulose) and reduced graphite oxide electrodes.[16,18]

Since the above-described integrated devices are composed of two distinct sub-components, this review summarizes the state of the art of the carbon materials derived from biomass with a specific focus on the biomass conversion to activated carbon, and their applications as electrode material for SCs, DSCs and PSCs. Then in the last part the potential integration in one single power pack of hybrid solar cells with supercapacitors by sharing carbon electrodes is overviewed for low-cost sustainable energy technology.

2. CONVERSION OF BIOMASS INTO ACTIVATED CARBON

Due to remarkable properties, activated carbon (AC) is used in a wide range of applications.[19,20] As depicted in Figure 2 the interest for AC obtained from carbonaceous materials has risen every year. In this context, activated carbon is a form of carbon, obtained by a suitable treatment of raw materials to provide well-organized macro, meso and micro-pores and a wide range of chemical functional groups which can increase the surface area for adsorption or chemical reactions in the device.[21] Large varieties of carbon sources can be used, including fossil and biomass-based materials.[22,8] Traditionally, carbon materials were extracted from fossil resources such as coal.[22] However, global awareness of the environmental impacts and resources limitation has dramatically decreased the motivation for fossil-based material consumption. Therefore, biomass-derived materials, i.e., materials prepared from plants, living-organisms, plant or animal wastes, have attracted great interest for the synthesis of AC materials due to advantageous characteristics, as abundance, low-cost and easy conversion into conductive carbon, compared to other available

sources.[22,24] In addition, the use of residual biomass as low-cost option for production of ACs has gained more attention in recent years (Figure 2).

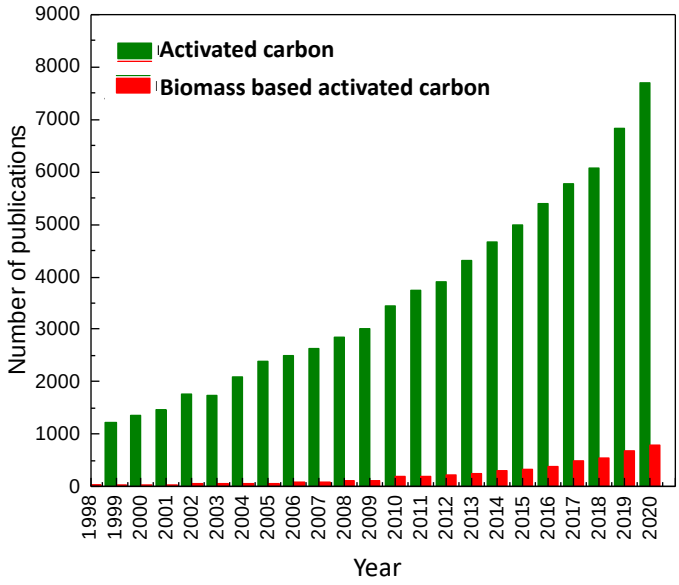

Figure 2. The number of publications on the activated carbon prepared from different carbonaceous precursors, data obtained using "activated carbon" and "biomass based activated carbon" keywords surveyed in Scopus database.

In a general way, activation process of carbon can be divided into two types, namely physical and chemical activation based on the types of activating agents. Further, these two activation processes can be carried out as single step activation or through a two steps process that are carbonization followed by activation.[25] During the carbonization process, carbon atoms are rearranged to give a graphitic like structures that creates the initial porosity of the carbonized material.[26] This initial porosity generally exhibits a very low surface area due to pore filling or blocking by deposition and decomposition of tars.[27] The final product of the carbonization process is named carbonized material, char or biochar, which is enriched in aromatic rings (Figure 3).

Through physical activation, biochar is further activated using steam, carbon dioxide, air or mixture of gases as activating agent at temperatures around 350-1000℃, which leads to an increase of the carbon porosity.[28] Generally, the activating agent is adsorbed and dissociates in the active sites of the carbon surfaces, generating gases which, in turn, can adsorb on the active sites, thus inhibiting them. The above reaction is reversible, and the active sites are continuously formed upon creation of the porosity.[29]

In the chemical activation process, organic precursors are activated in presence of activating agents such as NaOH, KOH, K_3CO_3 H_3PO_4 or $ZnCl_2$.[30] This activation process can be carried out directly from the raw biomass or carbonized biochar. First, activating agents are mixed with carbon samples to merge with the internal structure.[21] Depending on the activating agent, various reactions with complex mechanisms take place at higher temperatures with cellulose, hemicellulose and lignin contained in the carbon precursor. During the decomposition, activating agents act as dehydrating and oxidizing agents, thereby opening inaccessible pores, allowing the formation of new pores and/or enlarging existing pores while preventing the formation of tars and ash.[31] This process is carried out at relatively moderate temperatures (around 300–800 °C) depending on the precursor material. In the final step of chemical activation, AC is washed several times with water to remove the remaining traces of activating agent.[26] Figure 3 depicts the synthetic routes towards AC using different methods.

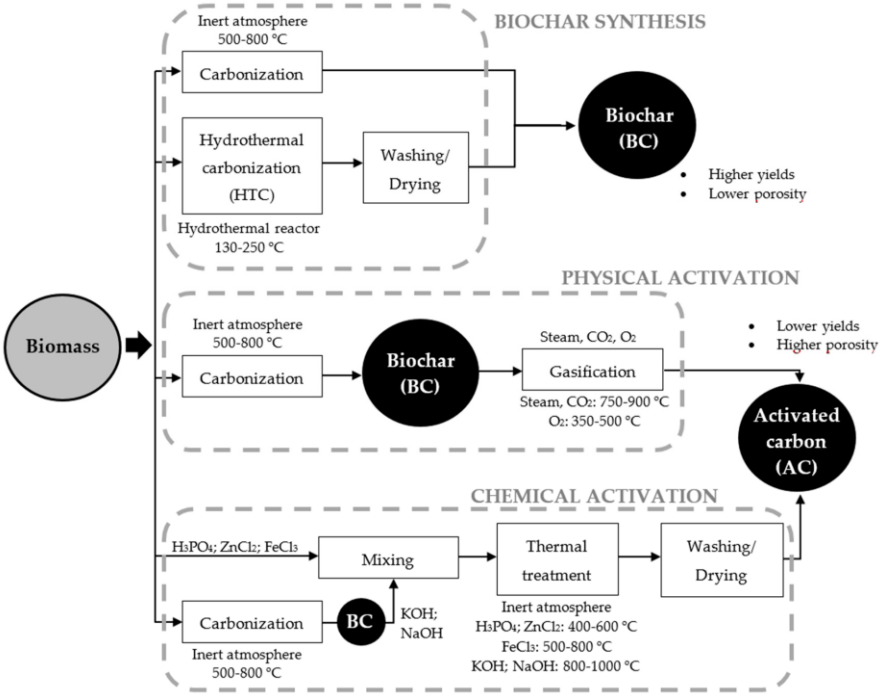

Figure 3. Synthetic routes towards activated carbon from biomass. Figure reproduced from Bedia et al.[25] with permission from MDPI.

As example, AC from rice husk was synthesized by Le Van et al. using NaOH as activating agent and different activation temperatures in the 650–800 °C range.[32] As the temperature increased, the surface area changed from 2482 to 2681 $m^2 g^{-1}$. This surface increase was due to the formation of additional pores by volatile compounds release at high temperature.[33] However higher activation temperatures (above 900 °C) led to a decrease in the surface area, owing to structural changes including pore widening and blocking.[34] Furthermore, using H_3PO_4 as activation agent, Wu et al. reported AC surface area of 1252 $m^2 g^{-1}$ from Pomelo peel and 675 $m^2 g^{-1}$ from Arundo donax Linn.[35] The total pore volume and mean size for Pomelo peel and Arundo donax Linn were 1.33 cm^3, 4.26 nm and 0.31 cm^3, 1.85 nm, respectively. This work demonstrates that the precursor material has a huge impact on the surface area and pore size distribution of ACs.

Kumar et al. used Fox nutshell for the production of AC with $ZnCl_2$ as activating agent.[36] High surface area of 2869 m^2 g^{-1} was reached with total pore volume of 1.96 cm^3 g^{-1}. Three different types of AC were prepared by Gundogdu et al. by changing the ratio of $ZnCl_2$ and using tea wastes as biomass precursor.[37] This study reveals that the characteristics and porous structure may depend on the ratio between the starting material and the activating agent. On the other hand, Özsin et al. prepared AC from agricultural wastes of chickpea with K_2CO_3 and KOH as activating agents and different impregnation ratios.[38] At impregnation ratio of 50 wt.% using KOH, the AC showed highest surface area of 2082 m^2 g^{-1}, compared to 1921 m^2 g^{-1} for 75 wt.% using K_2CO_3. Figure 4 illustrates the diverse porosities reachable as a function of the activation procedure applied to a single precursor material (i.e., chickpea).

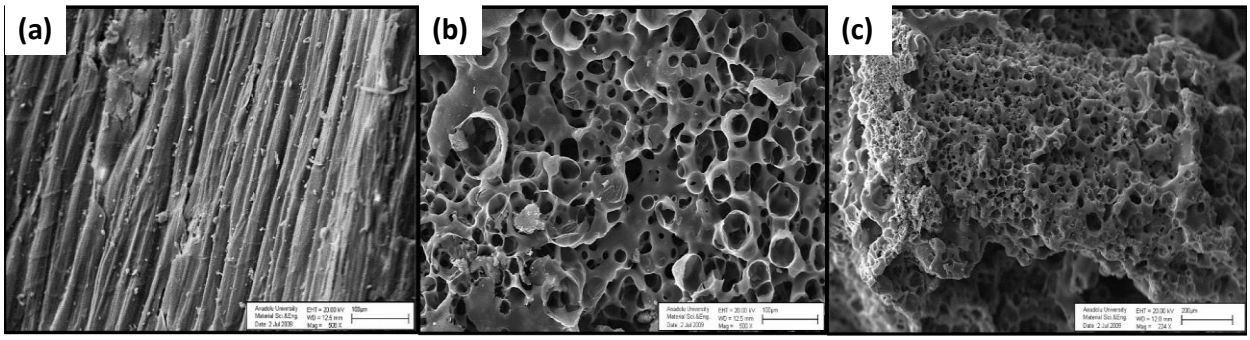

Figure 4. SEM images of a) raw chickpea straw, b) KOH activated carbon, and c) K_2CO_3 activated carbon. Figure reproduced from Özsin et. al. [38] with permission from Springer Nature.

The surface properties of activated carbon depend on the precursor material, activating agent and method of preparation. Therefore, depending on the application, ACs can be modified to improve certain properties by introducing functional groups to the carbon surface.[39] Heteroatom dopants can change the electronic properties of carbon by changing the Fermi level.[40] Chen et al.

prepared activated carbon for PSC applications by using phosphorus (P) or boron (B) dopants in order to enhance conductivity and hole transporting ability. P doped carbon shows n-type properties with better conductivity while B doped carbon acts as p-type material.[41] Kim et al. synthesized nitrogen (N) and sulfur (S) co-doped porous carbons using naturally doped anchovy fish as precursor, the final AC product showed higher catalytic activity for Co^{III} reduction in DSC applications.[42] At the same time B-, N- and P-doped activated carbon have shown synergic effects compared to the bare activated carbon by increasing wettability, charge transfer rate and high charge storage area in supercapacitor applications.[43] Certain biomass materials used as precursor for the synthesis of doped ACs naturally contains a uniform distribution of heteroatoms in the structure. For example, soybean precursors (milk, beans, dregs), bamboo, pine needles, banana peel, walnut, yogurt, egg white and shells of sea food are rich in nitrogen, while the fish skin, fish scales and human hair are rich is nitrogen and sulfur.[44] Thus, selection of the biomass precursors has a strong impact on the physicochemical properties of the obtained carbonaceous materials.

3. BIOMASS-DERIVED CARBON ELECTRODES FOR SUPERCAPACITORS

Supercapacitors (SCs) are a type of electrical energy storage devices where the electrical charge is stored at the electrode/electrolyte interface.[45] These devices have very large electrode surface area, which leads to an increase in the capacitance per unit of area. Compared to other available energy storage devices such as batteries and conventional capacitors, SCs are the best alternative energy storage device that can fill the gap with regards to fast power delivery or harvesting.[46] SCs are successfully used to open the heavy emergency exit of the Airbus A380, or involved in electric cars, buses and electric trains.[47,48] All the materials constituting SCs are key, such as, electrode morphology, type of current collectors, separators and electrolytes.[49,50] A typical structure of

symmetric SC is shown in Figure 5a.[51] Published articles over the past two decades indicate the possibility of using biomass-based activated carbon as electrode for supercapacitors (Figure 5b).

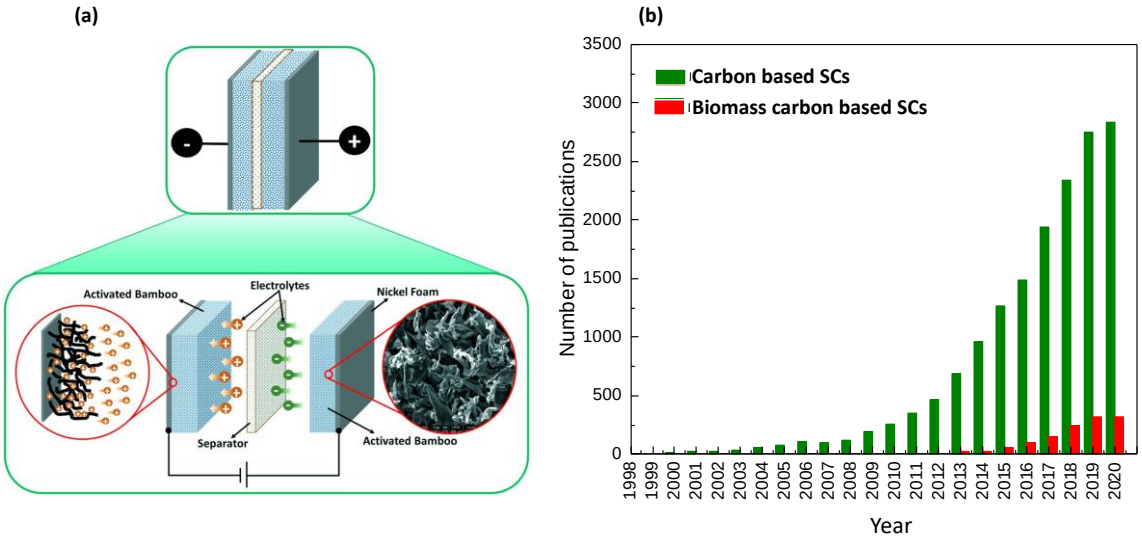

Figure 5. (a) Schematic representation of a supercapacitor and its components, carbon electrodes, separator and electrolyte. Figure reproduced from Zequine et al.[51] with permission from Springer Nature. (b) Literature survey using "activated carbon supercapacitors" and "biomass activated carbon supercapacitors" keywords in Scopus database.

The most commonly used materials for SC electrodes are based on carbon.[52] In particular AC shows suitable texture for the preparation of high-performance energy storage devices.[53-55]

In SCs the charge transfer mechanism strongly depends on the surface area accessible to electrolytic ions. Structural parameters such as pore size and shape, surface functionality and electrical conductivity play a key role in increasing the specific capacitance.[56] Among these factors, pore size has a significant contribution to determine the specific capacitance. The nature of the pore size distribution, more importantly the presence of both micropores and mesopores, rules the penetration or mobility of ions in the porous structure. Previous reports have shown that

mesoporous AC has a higher impact on ion diffusion than microporous one, because narrow micropores (0-1 nm) are not accessible to liquid electrolytes.[57] Some reports have shown good agreement between pore dimensions and electrolyte ion size.[58] However other studies have reported that micropores are highly desirable for increasing the specific capacitance.[59] Therefore, the ratio between the amount of micropores and mesopores should be controlled to obtain the highest capacitance.

The characteristics and storage properties of AC prepared from different biomass precursors are summarized in Table 1. Electrochemical performances of SCs are determined using most frequently the cyclic voltammetry and constant current charge/discharge technique. Evaluation methods and formulas for calculation of charge stored (capacitance, energy and power densities) in supercapacitors are detailed in the supporting information and Table S1.

Table 1 Textural and storage properties of activated carbons prepared from biomass precursors. V_{micro} and V_{meso}: microporous and mesoporous volumes; C_s: specific capacitance; E: specific energy.

Precursors	BET area ($m^2\ g^{-1}$)	V_{micro} ($cm^3\ g^{-1}$)	V_{meso} ($cm^3\ g^{-1}$)	Electrolyte	C_S ($F\ g^{-1}$)	E ($Wh\ kg^{-1}$)	Ref.
Aqueous electrolyte							
Rice husk	2121	0.59	0.24	6M KOH	123		67
	2696	0.27	0.69		147	5.11	
	1592	0.05	1.05		80		
Coconut shell	826	0.28	0.11		209		4
	1132	0.33	0.39		219		

	1532	0.32	0.89		228	38.5	
Banana stem	567.36	0.175	-		479.23		[53]
Argan seed shells	2062	0.95	1.04	1M H_2SO_4	355		[69]
	1654	0.62	0.58		259		
Lotus leaf	2297	0.73	-	6M KOH	379	9.2	[60]
	2488	0.61	-		274		
Willow Wood	2793	0.83	0.60		394	23	[5]
Organic electrolytes and ionic liquids							
Shaddock endotheliums	1265	0.58	0.13	1M $BMIMBF_4$/AN	99	46.88	[61]
Hemp stem	2801	0.53	1.18	1.8M $TEMABF_4$/PC	167	19.8	[62]
	2879	0.86	0.30		144		
Cherry stones	1167	0.56	-	1M $TEABF_4$/AN	110		[63]
	1624	0.67	-		119		
Pine tree powder	2207	0.42	0.99	$EMIMBF_4$	224	92	[64]
Aloe leaf	1890	-	-		126	40	[65]
Coconut shell	1998	-	-	MPPyFSI	219.4	92.1	[66]

As example, Teo et al. fabricated SCs using rice husk ACs showing specific surface area of 2121, 2696 and 1592 $m^2\ g^{-1}$ for activation temperature of 750, 850 and 950 °C, respectively.[67] Maximum surface area of 2696 $m^2\ g^{-1}$ and capacitance of 147 F g^{-1} were obtained after activation at 850 °C. The micropore volume was then reduced while increasing the mesopore volume. However, the highest pore volume and the specific capacitance were obtained at moderate micro and meso volumes.

Besides, the dependence of electrochemical performance on the presence of mesopores was studied by Mi et al. using coconut shell AC with well-controlled micro- and mesoporosity obtained by steam activation.[4] The mesoporosity was continuously developed with increasing the steam flow rate while maintaining almost the same micropore volume. Capacitance of each sample was almost equivalent which indicates that the micropores act as main charge storage space. In addition, this study revealed that mesopores are responsible for improved ion diffusion and reduce the internal cell resistance. Rufford et al. used charge-discharge cycles to determine the influence of meso- and micropores on the capacitance by charge-discharge rates.[68] This study showed that mesopores have more contribution to the capacitance at fast discharge rates compared to micropores. Elmouwahidi et al. synthesized AC using argan seed shells and the capacitance retention was tested with different current loads.[69] Nitrogen-rich AC showed the highest capacitance of 355 F g^{-1} at 125 mA g^{-1} while maintaining 93% of its capacitance at high current load (1 A g^{-1}). Also, high mesoporous structure has a contribution to retain its capacitance at high current loads. However, oxygen-rich AC led to capacitance of 259 F g^{-1} at 125 mA g^{-1} while maintaining 52% of its capacitance at high current load (1 A g^{-1}) because carboxyl groups at the surface reduce the electrolyte diffusion into the pores. These findings underline the key role of carbon material surface groups on the capacitance values.

In order to reach high storage performance, electrolyte plays a key role and must fulfill some requirements that are wide potential window, high electrochemical stability, high conductivity, environmental friendliness and low-cost.[70, 71] SCs with aqueous electrolytes exhibit high conductance and capacitance compared to organic electrolytes and ionic liquids. On the other hand, the operating potential window is low in aqueous electrolytes (< 1.2 V) compared to organic electrolytes and ionic liquids (over 3 V). Thus, ionic liquid SCs have higher energy densities,

because a wide operating potential has more impact on the specific energy of the device.[61,64-66] Although most commercially available SCs contain organic electrolytes, ionic liquid-based SCs have recently grained much attention to overcome the drawbacks of organic electrolytes such as volatility and inflammability.[72,73] Yet, to improve ionic conductivity the ionic liquids are usually mixed up with solvents. As an example, Yang et al. employed 1-butyl-3-methylimidazolium tetrafluoroborate/acetonitrile ($BMIMBF_4$/AN) electrolyte and capacitance of 99 F g^{-1} was obtained for SCs made of ACs synthesized from waste shaddock endotheliums.[61] This device showed outstanding performance with specific energy of 46.88 Wh kg^{-1} and over 93.7 % capacity retention after 10000 cycles which is rarely achieved by SCs employing biomass-sourced carbon materials. Nevertheless, the presence of solvent can lead to electrolyte leakage which affects the stability of the SCs. In order to solve this stability issue solvent-free ionic liquids are also used as electrolyte in SCs. As examples, SCs using solvent-free ionic liquid, as 1-ethyl-3-methylimidazolium tetrafluoroborate ($EMIMBF_4$) and 1-methyl-1-propy-pyrrolizinium bis(fluorosulfonyl)imide (MPPyFSI), were developed by several groups,[64-66] leading to devices with good specific energy (over 90 Wh kg^{-1}). Karnan et al. used AC prepared from Aloe leaf and capacitance of 306 F g^{-1} was achieved for devices using aqueous 1M H_2SO_4, 244 F g^{-1} using gel-type polyvinyl alcohol (PVA)/H_2SO_4 and 126 F g^{-1} using non-volatile ionic liquid $EMIMBF_4$.[65] It is also worth mentioning that the maximum specific energy of the aqueous electrolyte-based device was about 15 Wh kg^{-1} while over 40 Wh kg^{-1} was obtained with ionic liquid. Therefore, the ionic liquid SCs provide wide potential windows with higher specific energy.

4. BIOMASS-DERIVED CARBON ELECETRODES FOR HYBRID SOLAR CELLS

Owing to its low manufacturing cost, the PSC technology, derived from DSCs, is the most promising next generation alternative to conventional silicon-based cells.[74,75]

In brief, the first concept of electricity generation from dyes chemisorbed onto metal oxide electrodes in an electrochemical cell was introduced by Gerisher et al. in 1968.[76] In 1991, to adsorb larger dye amounts, O'Regan et al. proposed the use of mesoporous TiO_2 films showing a surface area several orders of magnitude higher than dense oxide film.[74] This solar cell technology, allowed the development of DSCs with PCE of 14.3% (published) and 13.0% (certified by Newport).[77-79] Due to the volatile solvents involved in DSCs, which greatly affect the stability and production of the cells, Bach et al. proposed in 1998, solid-type hole transport materials (HTM) e.g. spiro-OMeTAD.[80] Extensive work has been done for the solidification of the DSCs electrolyte, and PCE up to 7.2% was reported which remained lower than that of liquid-DSCs.[81]

In order to reach higher PCE with solid-state DSCs, Kojima et al. proposed in 2009 to use hybrid perovskite, i.e., $CH_3NH_3PbI_3$ (or $MAPbI_3$) and $CH_3NH_3PbBr_3$ (or $MAPbBr_3$), as a new light–absorber. However, the devices initially showed poor stability due to the dissolution of the perovskite material in liquid electrolytes.[75] As at the same time, Spriro-OMeTAD had become familiar as hole transport material for solidification of DSCs, it was also applied as solid electrolyte to solve the stability issue of the hybrid perovskite. The PCE of solar cells therefore significantly increased up to 9.7%.[82] Since then, remarkable improvements have been achieved and PCE of perovskite solar cells increased up to 25.5% as recently certified.[79] According to the theoretical calculations, this material has the potential to achieve efficiencies as high as 31% in single junction and over 40% in tandem configuration with silicon-solar cells.[79,83,84] Extensive works were carried out in this field to improve the efficiency, stability under real conditions and fabrication cost of PSCs. In this regard, as low-cost and long-term stability devices the carbon-PSCs are recognized as extremely appealing candidates for practical applications. Carbon electrode materials derived from biomass have been proposed as promising candidate for hybrid solar cells. Figure 6 illustrates

the evolution of the research in the field of DSCs and the number of papers published on the hybrid solar cells with standard and carbon-based configurations.

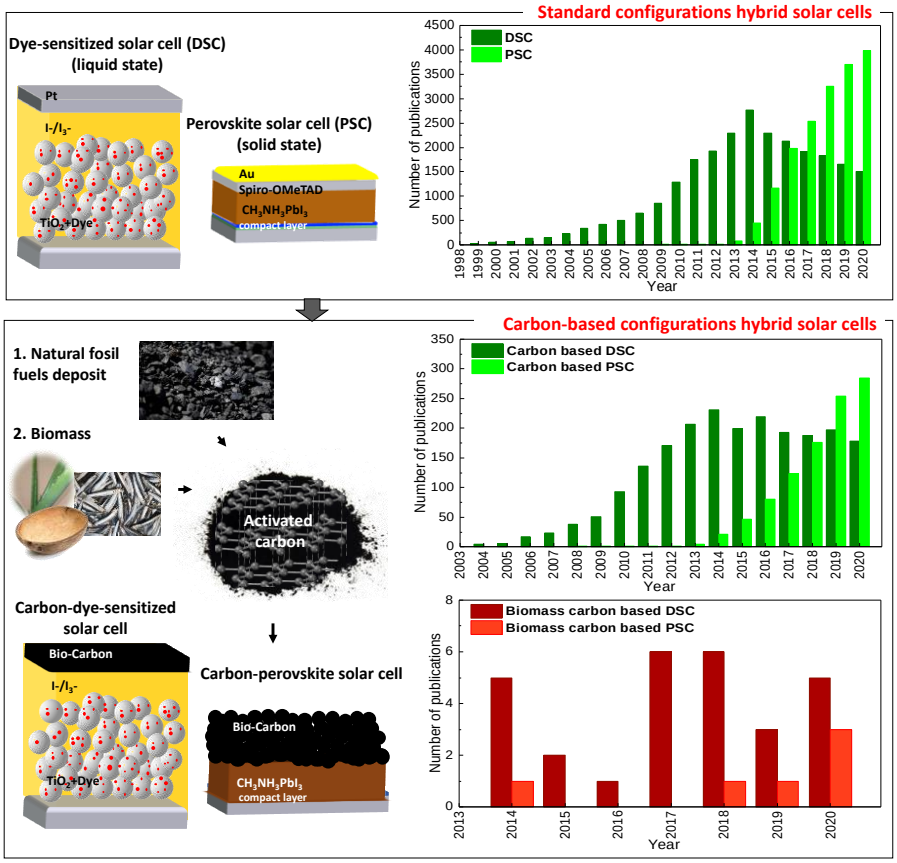

Figure 6. Evolution of the research works in the field of dye-sensitized and perovskite solar cells, from conventional approaches to bio-sourced carbon-based solar cells, reports published over years found in Scopus database using "carbon and biomass carbon" for "dye-sensitized solar cells, and perovskite solar cells" as keywords.

In the next sections, we will describe the research work reported so far towards the replacement of expensive counter-electrodes by biomass derived carbon electrodes for stable and low-cost DSCs and PSCs.

4.1 DYE-SENSITIZED SOLAR CELLS

DSC counter-electrodes should fulfill several requirements such as a good catalytic activity, long-term thermal and chemical stabilities, and high conductivity. Various types of carbon materials such as carbon black, graphene or carbon nanotubes were used as back-contact in DSCs and PSCs.[85-102] It should be noted that the champion DSC structure involves mesoporous TiO_2 sensitized with ADEKA-1/LEG4 dyes, $Co^{III/II}$ couple as redox electrolyte and a graphene nanoplate-based counter-electrode (GNP). This system allowed to obtain a PCE of 14.3%, which remains the highest values reported since 2015.[77] It was observed that implementation of graphene as counter-electrode produces higher PCE, J_{sc} and FF than pure Pt electrodes. For comparison, a PCE value of 12.25% was reported in 2019 for devices using Y123 dye, $Co^{III/II}$ electrolyte and standard Pt counter-electrode.[78,79] Recently, the certified PCE value of DSCs was updated to 13.0%.[103]

Activated carbon (AC) is another candidate to replace the platinum counter-electrodes in DSCs. Extensive works were thus devoted on this direction that are reflected in the number of publications in the last few years as presented in Figure 6. Only 28 reports are published on the application of ACs extracted from biomass waste as counter-electrode for DSCs and the highest results of PCE are summarized in Table 2. [104-113] Highly conductive porous AC can be obtained from biomass with the use of simple activation methods already discussed in the first section and the resulting materials applied as low-cost counter-electrodes for high performance DSCs.

Table 2 Photovoltaic parameters of DSCs with biomass-derived carbon material as counter-electrode and corresponding power conversion efficiencies. The efficiencies of standard Pt-based DSCs are given in brackets.

Biomass precursor	DSCs structure	J_{sc}, mA cm^{-2}	V_{oc}, V	FF, -	$PCE^{C\ (Pt)}$,%	Ref.
Pomelo peel	FTO/mp-TiO_2/N719/I_3^-:I^-/AC	16.24	0.79	0.65	8.29 (8.24)	[104]
		14.65	0.81	0.67	7.81 (8.24)	[105]
Coconut shell		19.49	0.65	0.62	7.85 (9.41)	[106]
Bagasse	FTO/mp-TiO_2/N719/I_3^-:I^-/N-AC:Pt	15.3	0.73	0.62	6.98 (6.08)	[107]
Pine cone flower	FTO/mp-TiO_2/N719/I_3^-:I^-/AC	13.51	0.71	0.52	4.98 (6.25)	[108]
Coffee	FTO/mp-TiO_2/N719/I_3^-:I^-/N-AC	15.09	0.76	0.726	8.32 (8.07)	[109]
Fish scales	FTO/mp-TiO_2/N3/I_3^-:I^-/AC	15.64	0.75	0.66	7.83 (8.34)	[110]
Fish (anchovy)	FTO/mp-TiO_2/SM-315/ $Co^{III/II}$ /N,S co-doped-AC	18.78	0.89	0.75	12.72 (12.23)	[42]
Quince leave	FTO/mp-TiO_2/N719/I_3^-:I^-/AC	14.99	0.70	0.526	5.52 (6.56)	[111]
Aloe peel	FTO/mp-TiO_2/N719/I_3^-:I^- /AC:$NiWO_4$	14.70	0.70	0.69	7.08 (6.46)	[112]
	FTO/mp-TiO_2/N719/I_3^-:I^- /AC:$CoWO_4$	13.96	0.69	0.63	6.07 (6.46)	
	FTO/mp-TiO_2/N719/I_3^-:I^- /AC:$FeWO_4$	14.38	0.68	0.55	5.38 (6.46)	
Eggshell membrane	FTO/mp-TiO_2/N719/I_3^-:I^-/AC	13.40	0.79	0.63	6.71 (6.63)	[113]

notes: meso-porous, mp-; activated carbon, AC.

As an example, Jing et al. proposed the activation of carbon extracted from Pomelo peel by means of $ZnCl_2$ combined with post-carbonization.[104] It was found that catalytic activity significantly increased by including a small amount of self-doping heteroatoms such as N, P, S and Na, Mg, K, Ca, Fe, etc. leading to a homogeneous co-doping in one-carbon matrix structure. The DSCs with carbon-based electrode yielded a PCE of 8.29% which was comparable to that using Pt electrode

(8.24%). Later, the same group proposed a self-activation method, eliminating the use of $ZnCl_2$ as activation agent.[105] The solar cell based on this carbon-electrode reached 7.81% PCE, slightly lower than the previous report. In another study, Kumarasinghe et al. proposed an efficient method to produce highly conductive coconut shell charcoal using water activation agent and applied, then, as carbon electrodes for DSCs.[106] Activated carbon from pine cone flowers, was obtained by Nagaraju et al. by using KOH as activation agent and then applied as counter-electrode material for DSCs.[108] This type of biomass was chosen because it is an abundant source of carbon from cellulose, hemicellulose, and lignin. Additionally, the precursor material is a highly porous pulverized powder facilitating the absorption of ionic species K^+ and OH^- ions during the activation process. To fabricate homogeneous electrodes, a paste containing AC, carbon black, polyvinylidene fluoride (PVDF) as binder and N-methylpyrrolidone (NMP) as solvent was coated on FTO substrates and then dried at 80 °C for 6 hours. The DSCs with this type of biomass-based AC electrodes exhibited a PCE of 4.98%, value higher than that measured for commercial AC counter-electrode (4.45%). To generate effective porous structure, Chung et al. proposed a facile and effective method to prepare porous carbon by carbonization of earth-abundant coffee waste using $ZnCl_2$ activation.[109] Carbon paste was sprayed on top of FTO substrates and heated at 400 °C for 3 hours under Ar flow. A good PCE of 8.32% was obtained for DSCs using the AC electrode, value higher than that of conventional Pt-based electrode (8.07%). Fish waste is also abundant in nitrogen, sulfur, phosphorous elements, and contains high content of carbon.[110,42] Ma et al. achieved the carbonization of fish waste and the resulting material was used as counter-electrode in DSCs.[110] Using a simple carbonization method and KOH as activation agent, the resulting carbon material showed a large surface area (2933 $m^2 g^{-1}$) with high catalytic activity. As a result, the corresponding device exhibited a PCE of 7.83% with V_{oc} = 0.750 V, J_{sc}=15.64 mA

$cm^{-2,}$ and FF=0.668. Optimized carbon-based device performances are comparable to conventional Pt electrode device, with PCE=8.34%, J_{sc} =15.98 mA cm^{-2}, V_{oc} = 0.755 V, and FF = 0.691. From the CV analysis, the cathodic and anodic current density remain 90% of their initial values after 100 scanning cycles, demonstrating good stability against corrosive I^-:I_3^- redox couple electrolyte. Kim et al. used anchovy fish as biomass resource to synthesize nitrogen and sulfur co-doped porous carbon by carbonization at 700–900 °C and activation with KOH (Figure 7).[42] On the other hand, carbon electrodes annealed at 900 °C in combination with SM-315 sensitizer and a cobalt redox couple, led to 12.72% PCE compared to 12.23% for Pt-DSCs. According to electrochemical impedance studies, the R_{ct} of Pt and carbon-based electrodes were estimated to be 14.71 Ω and 7.56 Ω respectively. The lower R_{ct} indicates that the carbon-based electrode has a higher electrocatalytic activity for Co^{3+} reduction at the counter-electrode/electrolyte interface.

Figure 7. (a) Preparation of anchovy-derived nitrogen and sulfur co-doped carbon materials, and (b) the J-V curves of the DSCs with Pt (black curve) and AnC (N,S co-doped-AC) counter-electrodes (red curve). Figure reproduced from Kim et al.[42] with permission from Royal Society of Chemistry.

For recycling of fallen leaves, Cha et al. used KOH activation agent during the carbonization to produce porous carbon.[111] With AC prepared at optimized pyrolysis temperature of 800 °C, the carbon-based DSCs showed the highest current density (14.99 mA cm^{-2}) and PCE (5.52%) among other carbon-based electrodes, values comparable to Pt-based electrodes. Zhang et al. used Aloe peel to prepare carbon-MWO_3 oxide (MWO_4 with M = Fe, Co, and Ni) composite electrodes through hydrothermal method.[112] Among all composites, C-$NiWO_4$ exhibited excellent electrocatalytic activity for I_3^- reduction and fast electron transport capability. According to impedance measurements the charge-transfer resistance was reduced from 11.27 Ω to 2.17 Ω when $NiWO_4$ is integrated with carbon. The DSCs with C-$NiWO_4$ achieved a PCE of 7.08% surpassing that of Pt-electrode DSCs (6.46%). Moreover, these devices illustrated high stability in the redox electrolyte at different CV scans.

It was proved by Wang et al. that eggshell membranes can be recycled from domestic waste to prepare a unique micropore-rich carbon powder by carbonization.[113] The carbonized eggshell membranes were obtained by immersing the fresh eggshell into a sucrose solution and then carbonized at 800 °C. The resulting film of carbon prepared by doctor blade method and annealed at 350 °C led to 6.71% PCE in DSCs, comparable to that obtained with Pt-based counter-electrode (6.63%). Among photovoltaic parameters, V_{oc} of the carbon-based devices showed significant improvement from 736 to 795 mV. This increase was attributed to the positive potential shift of the redox couple relative to the Fermi level of TiO_2. However, J_{sc} of Pt electrode was slightly higher (13.78 mA cm^{-2}) due to the better reflectance than that of carbon electrodes (13.40 mA cm^{-2}). The higher FF of 0.65 obtained for Pt electrode DSCs was attributed to its lower resistance compared to carbon-electrodes (FF of 0.63). As a result, the increased PCE of the carbon-based DSCs was related to the significant change in V_{oc}.

4.2 PEROVSKITE SOLAR CELLS

In contrast to DSCs, PSC counter-electrode does not require any electrocatalytic activity. In a device involving hole transport material, the work function of counter-electrode materials should be higher than the Fermi level of the p-type layer. Moreover, electric conductivity and morphology of the interface with perovskite is crucial for high performance and long-term stability PSCs. To date, the most popular counter-electrodes for PSCs are noble metals like gold (Au) or silver (Ag). Apart from high materials cost, interfacial degradation due to the metal electrodes has been widely discussed as a major issue preventing PSCs development. It was mentioned that the Au migration through the HTM into perovskite leads to a serious issue for device stability.[114] On the other hand, Ag tends to react with the perovskite layer leading to its degradation.[115] It has been already demonstrated that carbon makes PSCs more stable without using any special sealant.[116] A variety of carbon materials has been adopted to replace noble metals and many kinds of perovskite solar cell structures were proposed. [117-136] Carbon can indeed play double function, i.e., HTM and back-contact electrode.

To date, the most performing standard PSC configuration shows a certified PCE of 25.5% (24.82% published).[79,137] For carbon-based PSCs the highest reported values is 15.7 % for ZrO_2/C back-electrode configuration (Table 3).[138] These remarkable efficiencies are due to the perovskite layer optoelectronic properties and optimized cell structures together with finely tuned interfaces.[138,139]

Table 3 Record PCE (published and certified) of PSCs.

PSCs structure	J_{sc}, mA cm^{-2}	V_{oc}, V	FF, -	PCE, %	Ref.
FTO/c-TiO_2/mp-TiO_2/α-$FAPbI_3$:(MA:Cs)/spiro-OMeTAD/Au	26.35	1.164	0.809	24.82*	[137]
FTO/c-TiO_2/mp-TiO_2/$FAPbI_3$/spiro-OMeTAD/Au	25.74	1.1885	0.832	25.5**	[79]
FTO/c-TiO_2/mp-TiO_2/ 1.2 μm ZrO_2/C-O/$(5\text{-AVA})_xMA_{1-x}PbI_3$	23.2	0.980	0.69	15.7*	[138]

*published value, ** certified value by Newport; notes: meso-porous, mp-.

As ultra-low-cost carbon materials, biomass can be considered as one of the most important precursor sources. The number of research papers for the application of biomass as low-cost carbon source for carbon-based PSCs is still limited compared to those dealing with carbon-DSCs. From careful literature survey (Table 4), only five papers were found with a detailed analysis of the carbon materials obtained from biomass as electrode for PSCs. For instance, carbon materials derived from Aloe Vera plant (AV-C) was used as counter-electrode for PSCs.[140] First the Aloe vera gel was removed from leaves and dried under sunlight for 1 day. The dry material was further treated under an oil lamp for one night and thereby converted into black powder, that was finally ground by ball milling.

Table 4 Configuration and photovoltaic parameters of biomass-carbon electrodes for PSCs.

Biomass precursors	PSCs structure	J_{sc}, mA cm^{-2}	V_{oc}, V	FF, -	PCE, %	Ref.
Aloe vera plant (AV)	FTO/c-TiO_2/mp-TiO_2/$MAPbI_{3-x}Cl_x$/AV-C	15.22	0.953	0.50	7.25	[140]
	FTO/c-TiO_2/mp-TiO_2/ZrO_2/$MAPbI_3$/AV-C	18.05	0.838	0.35	5.29	
	FTO/c-TiO_2/mp-TiO_2/ZrO_2/$MAPbI_3^{DC}$/AV-C	21.65	0.985	0.59	12.48	
Coconut shell	FTO/mp-TiO_2/$MAPbI_3$/AC	1.18*	0.220	0.28	~0.4	[141]
	FTO/mp-TiO_2/$MAPbI_3$/AC-Paraffin oil	2.55*	0.70	0.371	~4	
Waste plant (Eichhornia Crassipes, EC)	FTO/c-TiO_2/mp-TiO_2/$MAPbI_{3-x}Cl_x$/EC-GC4	22.01	0.631	0.43	5.97	[142]
	FTO/c-TiO_2/mp-TiO_2/$MAPbI_{3-x}Cl_x$/EC-GC8	21.96	0.620	0.468	6.38	
	FTO/c-TiO_2/mp-TiO_2/$MAPbI_{3-x}Cl_x$/EC-GC10	23.49	0.672	0.54	8.52	
Soybeam dregs (SD) conductive carbon (CC)	FTO/c-TiO_2/mp-TiO_2/$MAPbI_3$/K-SD_1-CC	21.75	0.94	0.59	12.05	[143]
Bamboo-chopsticks (BC)	FTO/c-TiO_2/mp-TiO_2/$Cs_{0.05}(FA_{0.83}MA_{0.17})_{0.95}Pb(I_{0.83}Br_{0.17})_3$/AC	23.15	0.85	0.65	12.82	[144]
Peanut shell (PS)		21.06	0.81	0.61	10.30	
Phragmites australis (PA)		19.35	0.74	0.54	7.85	
Corn stalk (CS)		18.70	0.69	0.49	6.36	

*In this case the value corresponds to I_{sc}(mA); notes: compact, c-; meso-porous, mp-.

The black powder was washed with 2M HCl and treated at 1000 °C to get activated. The fine ball-milled AC powder was mixed with CH_3NH_3I and chlorobenzene to yield a viscous paste that

was applied onto the doctor-bladed meso-TiO_2 layer drying at 130 °C for 30 min. The best device exhibited V_{oc}=0.953 V, J_{sc}=15.22 mA cm^{-2} and FF=0.50, leading to overall PCE=7.25%. In another design, a ZrO_2 insulating layer was added onto the mesoporous TiO_2 layer by spin-coating and then doctor-bladed on top the AV-C. In this case, the optimized device showed V_{oc}=0.838 V, J_{sc}=18.05 mA cm^{-2}, and FF=0.35, with a PCE of 5.29%. The low FF was attributed to the insufficient thickness of the TiO_2/ZrO_2 layer. To control the thickness, screen-printing method was applied to prepare triple layer-based scaffold mp-TiO_2/ZrO_2/AV-C. Then the hybrid perovskite precursor was dripped into mesoscopic layers. The optimized AV-C-based device yielded a V_{oc}=0.985 V, J_{sc}=21.65 mA cm^{-2}, FF=0.59, leading to improved PCE of 12.48%. Un-encapsulated devices involving ZrO_2 showed good stability and retained 85% of their initial efficiency after 1000 hours at 35% relative humidity.

Furthermore, coconut shell charcoal was proposed as abundant, cheap and environmentally-friendly precursor material for AC.[141] In order to enhance the adhesion of bio-carbon on the FTO substrates the carbon powder was mixed with paraffin oil. The paraffin oil gave a different texture of AC and enhanced the device PCE to about 4%, with V_{oc}=0.7 V, I_{sc}=2.55 mA, and FF=0.371. Using an invasive plant (Eichhornia Crassipes, EC), Pitchaiya et al. demonstrated facile preparation of porous graphitic carbon (GC) which was readily used as efficient hole transport and back-contact electrode material, thus playing a dual role in PSCs.[142] Graphitization and conductivity of the carbon material were improved at three different annealing temperatures (450, 850, and 1000 °C, named EC-G4, EC-G8 and EC-G10, respectively). The highest conductivity, i.e., 115.20 S cm^{-1}, was attained for the highest annealing temperature (1000 °C) compared to 67.33 and 68.05 S cm^{-1} for 450 °C and 850 °C, respectively and a surface area of 1000.45 m^2 g^{-1} was obtained for the sample annealed at 1000 °C. The device made with EC-GC10 yielded a PCE

of 8.52% with J_{sc}=23.49 mA cm^{-2}, V_{oc}=0.672 V and FF=0.54. The other two devices, built with EC-GC4 and EC-GC8, exhibited PCE of 5.97% and 6.38%, respectively. The improved J_{sc} and FF obtained with EC-GC10 were attributed to enhanced graphitic phases and porosity of the material. Moreover, the champion device led to better air stability retaining up to 94% of its initial PCE value after 1000 hours under ambient conditions (25 ± 5 °C and 70 ± 5% relative humidity).

A large surface area of 1379 cm^2 g^{-1} was obtained with the AC from soybean dregs using KOH as activation agent.[143] In this case, it was observed that using an AC/conductive carbon composite, the perovskite/carbon composite interface quality, and charge transfer ability were greatly improved. Thus, used as back-electrode in carbon-based PSCs, the interface performance was significantly improved and a PCE of 12.05% was obtained, which is 50% higher than that of pure carbon-based PSCs.

Gao et al.[144] recently developed economical and eco-friendly bio-carbon PSCs using four different biomass precursors for the preparation of AC (Figure 8). The precursors are bamboo chopsticks, peanut shells, phragmites australis, and corn stalks. The biomass precursor was first dried, cut into pieces, carbonized at 1200 °C for 2h in a tube furnace, and the obtained carbon powder was ball-milled for 48h. The amount of carbon-produced by this method was 1.5 kg. The authors reported that the main carbon production cost was imputable to electricity consumption during carbonization. The specific consumption energy of 0.49$/kg was calculated. The overall performance of biomass-based PSCs depends on the morphology, interfacial connection, work function and sheet resistance of the bio-carbons. Bamboo chopstick AC showed better energy level alignment (suitable work function of 4.8 eV), lower radiative recombination and faster carrier transport. The mixture of bamboo-carbon material and acetylene black was sprayed or doctor bladed over the perovskite layer using chlorobenzene as solvent, and finally annealed at 90 °C.

The device exhibited a PCE of 12.82% maintaining 87% of the initial PCE after storage at room temperature for 2000 hours.

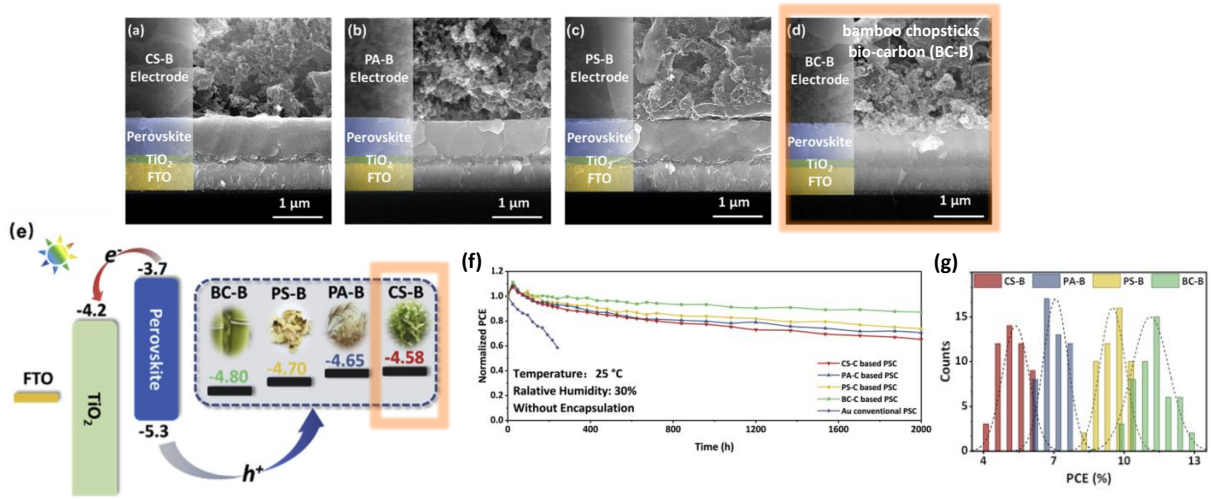

Figure 8. SEM images (a-d), energy level alignment (e), stability tests (f) and PCE histograms (g) of carbon-based PSCs. Figure reproduced from Gao et al.[144] with permission from Elsevier.

5. CARBON-BASED PHOTO-SUPERCAPACITORS

Thanks to the potential use of carbon electrodes in hybrid solar cells, DSCs and PSCs can be integrated with SCs. The interconnection can be categorized into two- and three-electrode systems. In DSCs, in order to avoid electrolyte penetration from the solar cell to the storage subcomponent, the use of an intermediate electrode was proposed. This allowed to solve the problem of device short-circuiting or supercapacitor self-discharging. The intermediate electrode can be based on different materials or material with different sides, one side being used as electrode for the solar cell and the other side as electrode for the supercapacitor. To design the photo-charging combined system using PSCs, the electrolyte and electrode materials of the subcomponent devices are also

important. On the one side, perovskite solar cells afforded high PCEs and high stability by using carbon layer as solid hole-transport material and back contact. On the other side, solid- or quasi-solid biomass carbon-based supercapacitors developed in the last decade can be potentially used on top of perovskite. Integration within two- or three-electrode systems using a shared electrode connecting both devices is very promising to save energy and improve device portability thanks to lower weight.

The operational mechanism of the integrated device can be described as follows: under illumination, electrons from the absorber are injected into the electron-acceptor material (TiO_2) and flow through the external circuit to the counter-electrode where negative charges are accumulated (Figure 9). At the same time the opposite electrode is used for accumulation of positive charges, negative ions of the electrolyte are then attracted toward this positive charges, and positive ions are attracted at the negatively charged electrode. This way, during the charging process, the separation of electrolyte ions is performed and a double layer is created, which reorganizes itself again during the discharge process.

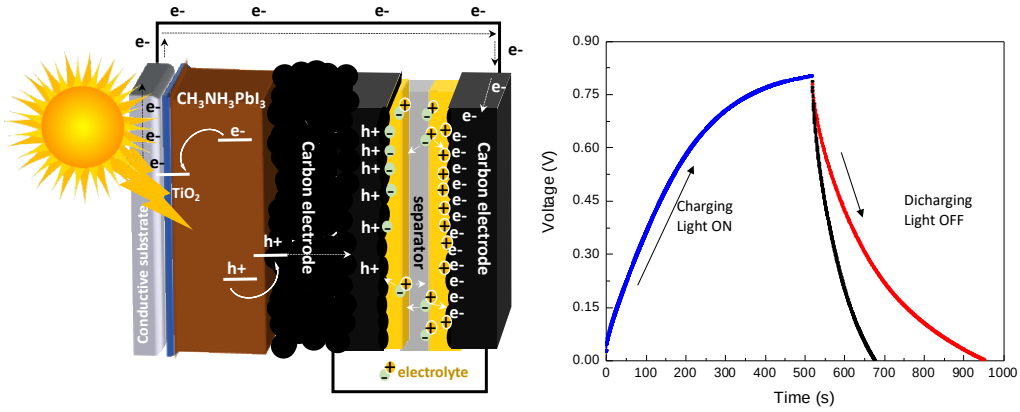

Figure 9. Working mechanism of the integrated energy conversion-storage device using PSCs.

The key parameters for the evaluation of integrated devices are overall efficiency and storage efficiency, extracted from the charge-discharge curves using direct device connection.[145,146] Detail of the evaluation process is included in the supporting information (Table S2).

Table 5 summarizes the record conversion-storage efficiencies reached for integrated devices using a shared carbon electrode. The best overall efficiency reported for DSC-integrated device is 5.12% with a storage efficiency of 84%, while the highest value to date for PSC-integrated device reached over 10% with supercapacitor based on C/polypyrrole (PPy) nanofibers/MWCNTs.[15,16] The integrated DSC and PSC device evaluation was performed for small active area, i.e., 0.36 and 0.06 cm^2, respectively. Recently, for a robust interconnection formed via electric glue and efficient PSCs with an area of 1 cm^2 the PSC/SCs integrated device exhibited an overall efficiency of 10.97% and storage efficiency of 80.31%. Those values are the highest reported for integrated self-charging power packs using inverted structure PSCs and supercapacitor based on reduced graphene oxide electrodes and polymer electrolyte (PVA/H_3PO_4).

Table 5 Best reported efficiencies for energy conversion-storage devices.

Solar cell structure	PCE,% (active area, cm^2)	Storage device structure	$\eta_{overall}$, $\eta_{storage}$ %	Ref.
DSCs: FTO/mp-TiO_2/N719/PVDF:I^-:I_3^-/ MWCNT	6.10 (0.36)	MWCNT/PVA-H_3PO_4/MWCNT	5.12, ~84	[15]
PSCs: FTO/c-TiO_2/mp-TiO_2/ $MAPbI_3$/spiro-OMeTAD/Au	12.6 (0.06)	MWCNT/PPy/ MWCNT	~10, ~50	[16]

ITO/PSS/PTAA/ $MAPbI_3/PC_{61}BM$/PEI/Ag	13.66 (1.0)	RGO/PVA/separator/PVA/ RGO	10.97, 80.31	[18]

notes: compact, c-; meso-porous, mp-.

As reference integrated system, Westover et al. have reported a storage efficiency of 84% (overall efficiency of 12.4%) for an integrated all-silicon solar cell/supercapacitor system with a solar cell operating at 14.8% PCE.[147] To the best of our knowledge this is the highest value ever reported for overall efficiency of solar cells integrated with SCs.

5.1 DYE-SENSITIZED SOLAR CELL/SUPERCAPACITOR

DSCs have demonstrated the ability to harvest light under critical conditions like during cloudy days or under diffuse light.[148,149] Due to the rapid growth of electronic equipment for Internet of Things, devices capable of self-charging own great potential for future application. In this section, we will focus on integrated conversion-and-storage devices using carbon-based shared electrodes (Table 6).

The first integrated DSC device was proposed by Miyasaka et al. in 2004.[150] Typical DSC made of a mesoporous TiO_2 layer sensitized with a ruthenium dye involved a platinum-coated AC counter-electrode to complete the device. The I^-/I_3^- redox electrolyte typically used in DSCs was replaced by a LiI hole-trapping layer covering TiO_2. The electrode materials of the AC-based SC were sandwiched and the gap was filled with an electrolyte solution containing 15% $TEABF_4$ in propylene carbonate (PC). After photon absorption by the dye, electron hole pairs are created. Following this, electrons are injected into the conduction band of TiO_2 transferred at the counter-electrode through the external circuit and accumulated at the surface of porous AC. At the same time, holes react with LiI layer and positive charges are trapped at the surface of AC as well. This integrated system achieved maximum charging voltage of 0.45 V, areal capacitance of 0.69 F cm^-

^{2} and charge-discharge coulombic efficiency of 80%. The limitation of this system stems from high internal resistance that retards the discharge process, during which electrons must overcome the Schottky barrier at the TiO_2 layer. Later, Nagai et al. proposed a new configuration by including an additional electrode to operate efficient charging by redox reaction.[151] Inspired by this work, Murakami et al. proposed in 2005 a three-electrode system including an internal bifunctional electrode between the working and counter-electrode which led to redox electron transfer on one side and charge storage on the other side.[152] This configuration afforded a large energy output of 47 μW h cm^{-2} (value five times higher than that obtained with the two-electrode system, 9.3 μW h cm^{-2}) with a high charge state voltage of 0.8 V. This improvement was attributed to efficient electron and hole transfer at the Pt/AC electrode.

Table 6 Photovoltaic performances of integrated dye-sensitized solar cell/storage device using carbon electrode as shared electrode.

DSCs structure	Inter-layer	PCE (%), (active area, cm^2)	Storage device structure	η_{ECSE} , $\eta_{storage}$ (%)	Ref.
FTO/mp-TiO_2/N719/LiI/AC:Pt	AC:Pt		AC/$(CH_3CH_2)_4NBF_4$:PC/AC		[150]
FTO/mp-TiO_2/N719/I^-:I_3^-/AC	Pt		AC/$TEABF_4$:PC/AC		[152]
FTO/mp-TiO_2/LEG4/ $Co^{III/II}$ / Ni(Co)O_x/Ni/PEDOT	Ni foil	4.9 (0.25)	Ni(Co)O_x/KOH/AC	0.6,-	[153]
FTO/NW-ZnO/N719/I^-:I_3^-/ ZnO:G	Cu mesh		ZnO:G/PVA-H_3PO_4/G		[154]

Wire-Ti/CNTs-TiO_2/N719/I^-:I_3^-	CNTs	2.20	TiO_2:CNT/PVA:H_3PO_4/TiO_2: CNT	1.5, 68.4	[155]
Wire-Ti/CNTs-TiO_2/N719/EMII-PMII:I^-:I_3^-	CNTs	2.73	TiO_2:CNT/PVA:H_3PO_4/TiO_2: CNT	2.1, 75.7	[156]
Ti fibers/TiO_2/N719/ EMII-PMII:I^-:I_3^-/ CNT	CNTs	6.47 (0.1214)	CNT/PVA:H_3PO_4/CNT	1.83,-	[157]
Ti/mp-TiO_2/N719/I^-:I_3^-/Pt	Pt	1.38 (0.22)	G/NaCl/G	1.02, 73.9	[158]
Ti/mp-TiO_2/N719/I^-:I_3^-/Pt	Pt	4.33 (2.5)	AC/NaCl/AC	3.72, 85.9	[159]
FTO/mp-TiO_2/Z907/I^-:I_3^-/Pt	Pt	2.25	AC/PEO:Pyr_{14}TFSI/AC	1.67, -	[160]
ITO-PEN/mp-TiO_2/N719/I^-:I_3^-/Pt	Pt	2.8 (0.16)	rGO/Polyurethane:RTIL/rGO	-	[161]

notes: meso-porous, mp-.

More recently, a liquid-type DSC using cobalt-based electrolyte and LEG4 dye was integrated with asymmetric $NiCoO_x$/AC-based SC to produce a photo-rechargeable integrated system able to generate and store energy.[153] Under open-circuit conditions the DSC provided a voltage of 0.8 V with PCE of 4.6-4.9%. The asymmetric stand-alone SC provided a specific capacitance of 46 F g^{-1} corresponding to energy and power densities of 4.1 Wh kg^{-1} and 41 W kg^{-1}. After integration of the two components, a specific energy of 2.3 Wh kg^{-1} (specific capacitance 32 F g^{-1}), coulombic and total efficiencies of 54% and 0.6%, respectively, were reported for the integrated system.

Due to the liquid solvent used in DSCs, the electrolyte can easily diffuse towards the storage part and thereby create short-circuits or fast self-discharging. Yang et al. proposed an all-solid-state flexible integrated device in which both free-standing solar cell and storage device were used in combination with aligned MWCNTs films as electrodes (Figure 10).[15]

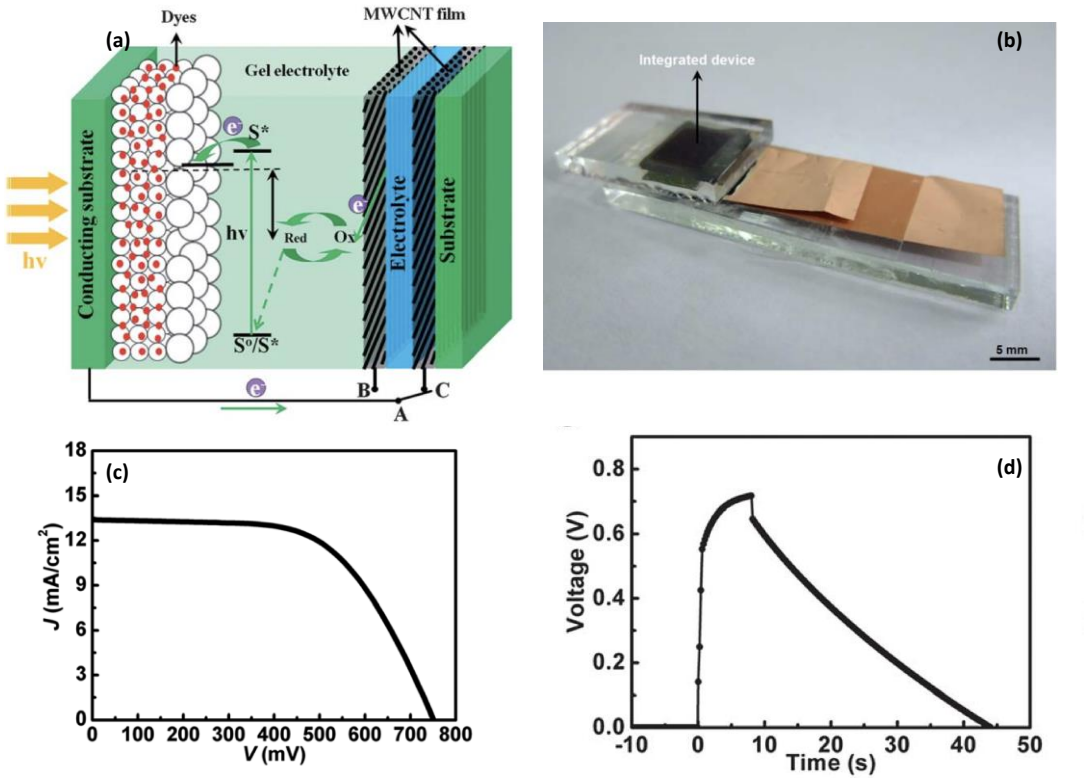

Figure 10. (a) Scheme of the integrated DSCs with storage device based on aligned MWCNTs films as electrodes, (b) photograph of integrated device, (c) J-V curve of DSCs, and (d) dynamic voltage during charging and discharging processes. Figure reproduced from Yang et al.[15] with permission from Royal Society of Chemistry.

PVA-H_3PO_4 electrolyte was used for the storage device and a gel electrolyte based on PVDF:I^-:I_3^- was used for the DSC. A PCE of 6.1% with V_{oc}=0.750 V, J_{sc}=13.41 mA cm^{-2} and FF=0.61 was registered for the corresponding DSCs using MWCNT-polyaniline (PANI) composite as counter-electrode. The specific capacitance of MWCNT-PANI composite SC was 83 F g^{-1}. After integration in one single device, an energy storage efficiency of 84% and overall photoelectric conversion of 5.12% was obtained for solidified type photo-SCs.[15]

On the other hand, Scalia et al. proposed a flexible integrated device composed of DSC and graphene-based capacitor.[158] The DSC and SC electrodes were made of titanium and stainless-steel grids. Methacrylate-based polymer electrolyte membrane (PEM) were used after activation by soaking in two different liquid electrolytes, i.e., methoxypropionitrile solution of NaI/I_2 for the DSC and aqueous NaCl solution for the capacitor. PEM was also selected as electrolyte separator, which guarantees sufficient ionic mobility at ambient temperature, high mechanical robustness and easy sealing of flexible devices. The performance of the flexible integrated device was tested under standard (1 Sun) illumination conditions leading to overall energy conversion of 1.02% and decreasing the light intensity to 0.3 Sun led to maximum storage efficiency of 1.46%. This work nonetheless highlighted the advantages of integrating DSCs and supercapacitors, notably their fabrication easiness, cost-effectiveness of the materials and device working under low light intensity conditions. These results hold very promising prospects for the industrial scale-up of such integrated device. Later the same group proposed a two electrodes flexible integrated device using newly developed polymer membrane made of two PEG poly(ethylene glycol)-based sections separated by a perfluorinated barrier.[159] One side of this membrane was adapted to enable iodine electrolyte diffusion in the DSC and the other side allowed the capacitor operation, thus using the same electrode for energy-conversion and storage. The organic solvent in DSC and aqueous electrolyte of the SC, could coexist in one single device thanks to the impermeable perfluorinated barrier layer. Overall efficiency of 3.72% with storage efficiency of 20 mC cm^{-2} at 3 mA was obtained for this system. To enhance the voltage, Scalia et al. reported a DSC module, i.e., 4 series cells, connected with all-solid-state SC based on commercial AC electrodes and PEO-Pyr_{14}TFSI electrolyte.[160] The two subcomponents were integrated into a single device by hot press method. The DSC module achieved a remarkably high photo-charging potential of 2.45 V. After full

charging, a capacity value over 0.017 mA h cm^{-2} was obtained for discharging at 1 mA, and overall efficiency of 1.67% was registered at maximum power generation of the DSC.

Furthermore, Bae et al.[154] proposed an innovative structure involving fiber-based electrodes, use of ZnO NWs, and graphene as active material and electrodes for energy harvesting- and storage devices. To improve the device efficiency further optimization is still needed for example by matching the pore size of the fiber-based material with the electrolyte ion size or by controlling the density of the ZnO NWs, which is believed to be critical to obtain high performance SCs.

Chen et al. proposed another design using titanium wire as precursor TiO_2 nanotubes.[155] Aligned CNTs fibers were twisted with a modified Ti wire to produce a wire-shaped integrated device that exhibited overall photoelectric conversion and storage efficiency of 1.5%. The same group further improved this design by solidification of the so-called "energy fiber device" using ionic liquid-based DSC and gel-electrolyte SCs.[156] A PCE of 2.73% was reported for the DSC while the energy storage efficiency reached 75.7% with specific capacitance up to 0.156 mF cm^{-1} and power density of 0.013 mW cm^{-1} at current of 50 μA. Then Yang et al. developed a coaxial energy elastic type fiber that converts solar energy into electric energy in its sheath and stores energy in its core using aligned carbon nanotubes sheets as electrodes.[157] The coaxial structure and aligned nanostructure at the interface of the electrode enable a high overall energy conversion (1.83%) which is maintained under bending and stretching. Those papers proved the possibility of fabricating energy fiber devices that can be woven into wearable, self-powering energy textiles.

Finally, full flexible printable DSC-SC system was designed by Dong et al. which was capable of efficiently charging a SC to 1.8 V by connecting three series DSCs.[161] Moreover, the performance of the lightweight integrated devices was found to be stable under various extreme bending and tilting conditions in an outdoor test. Under bending (90°) and different tilting

directions the voltage increased from 644 mV to 714 mV. This enhancement was attributed to several parameters, one being the deformation of the assembly that may improve the mechanical and electrical contacts at solid-solid interfaces in the device.

5.2 PEROVSKITE SOLAR CELL/ SUPERCAPACITOR

As low-cost, high-performance photovoltaics with long term stability, carbon-based PSCs are promising candidates as energy harvester part in integrated devices. An activated carbon layer can be easily fabricated and used as shared electrode between the two sub-devices in the integrated pack (Table 7). Moreover, PSCs has ability to harvest the light efficiently under low-light condition showing PCE and voltage higher than DSCs.[148,162] These properties of PSCs make them extremely interesting for broad range of indoor applications including also self-charging devices for Internet of Things.

Table 7 Photovoltaic parameters of integrated perovskite solar cell/storage device using a shared carbon electrode.

PSCs structure	Inter-connection	PCE,% (active area, cm^2)	Storage devices structure	η_{ECSE} , $\eta_{storage}$ %	Ref.
ITO/PEDOT:PSS/$MAPbI_{3-x}Cl_x$/$PC_{61}BM$/Al	Al/Cu wires	14.3 (0.20)	Ag:PI/SSG/PVA:H_2SO_4/SSG / Ag:PI	-	[163]
FTO/c-TiO_2/mp-TiO_2/ZrO_2/$MAPbI_3$/PEDOT:C	PEDOT:C	6.37 (0.07)	PEDOT:C/$LiClO_4$/PEDOT:C	4.70, 73.77	[164]
FTO/c-TiO_2/MWCNT/$MAPbI_3$/PMMA	PANI:CNTs	2.476 (1.0)	PANI-CNT/PVA:H_2SO_4/PANI-CNT	0.76, 70.9	[165]

FTO/c-TiO_2/mp-TiO_2/$MAPbI_3$/C	C	7.79 (0.071)	MnO_2:C/PVA-LiCl/C	5.26, 67.5	[166]
FTO/c-TiO_2/ mp-TiO_2/$CsPbBr_3$ /nano-C	nano-C	6.1 (0.1)	nano-C/Silica gel/nano-C	5.1, -	[167]

notes: meso-porous, mp-.

For the first time, Xu et al. integrated PSCs with MWCNTs-PPy-based SC in series connection (Figure 11).[16] The symmetric SC electrodes with two C/PPy nanofibers/MWCNTs films and cellulose acetate membrane as separator were assembled. The overall efficiency of 10% was reported for series connected PSC and SC. The authors reported a PCE of integrated devices of 20% which was obtained when the SC was completely charged. An open-circuit voltage of 1.45 V was registered, which represents a contribution from the SC and solar cells at the same time. The storage efficiencies of about 50% could be obtained by considering the PCE of integrated solar cells of 20% with the contribution from the charged SC.

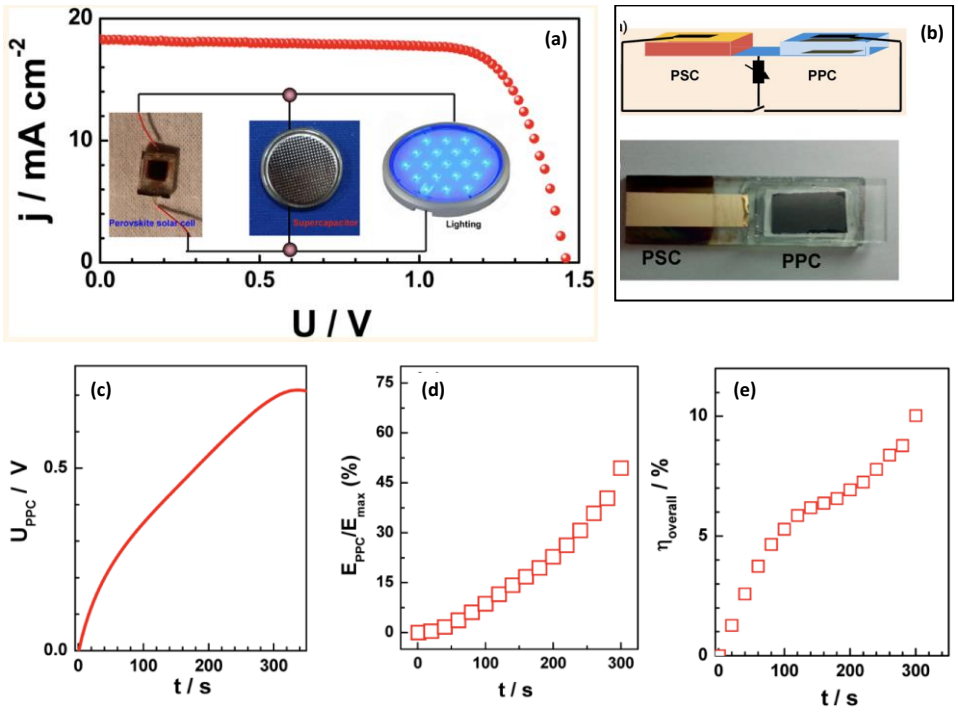

Figure 11. (a) Conceptual illustration, (b) Structural scheme of integrated energy pack containing PSC and PPy-based SC, and photograph of the integrated device, (c) charging curve of SC by the solar cell, (d) storage efficiency, and (e) overall efficiency versus time. Figure reproduced from Xu et al.[16] with permission from American Chemical Society.

A monolithic stacked PSC and solid-state SC was reported few years later (Figure 12). Overall efficiency of 10.97% and storage efficiency of 80.31% were obtained for integrated devices connected via electric glue with large-area inverted-configuration PSCs (1cm^2) and efficient SCs employing reduced graphene oxide electrodes coated with PVA/H_3PO_4 electrolyte.[18] Graphene oxide was prepared the pre-oxidation of a natural graphite commercial powder. To the best of our knowledge, this is by far the highest overall efficiency reported to date for integrated power pack.

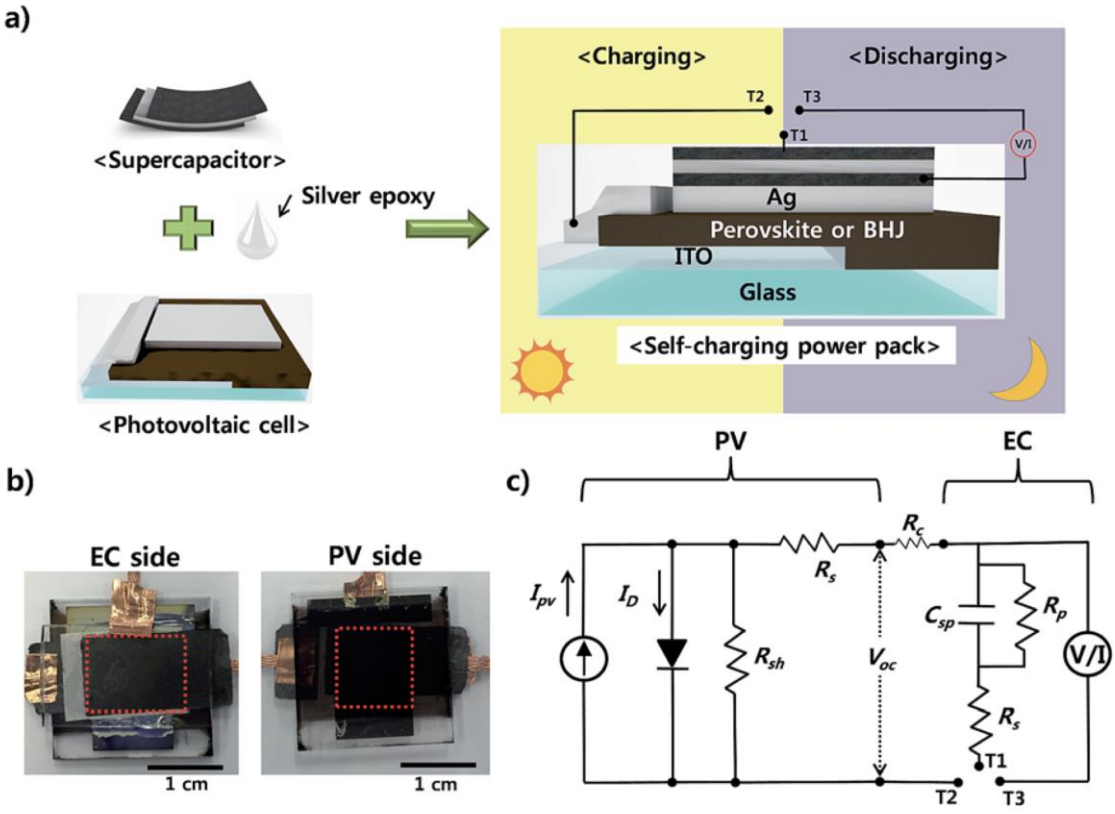

Figure 12. (a) Monolithic integrated energy pack containing PSC and RGO-based solid state SC, (b) SC and PSC sides photograph of integrated device, (c) equivalent circuit for integrated devices. Figure reproduced from Kim et al.[18] with permission from Royal Society of Chemistry.

Graphene electrodes were prepared by chemical converted graphene dispersion through facile vacuum filtration and implemented into semi-flexible integrated devices.[163] Natural graphite flakes were used as precursor, oxidized and then reduced by hydrazine hydrate in ammonia solution. Self-stacked solvated graphene (SSG) was coated on silver polyimide substrates, then H_2SO_4-PVA electrolyte gel was casted on top of the SSG-modified electrode and dried. Two electrodes were face-to-face assembled before performance assessment. The integrated device exhibited high specific capacitance of 245 F g^{-1} at 1 A g^{-1} and retained 83% of its original values after up to 10000

charge-discharge cycles. After integration of flexible SC with PSCs, a discharge voltage of 0.75 to 0 V was held for about 45s at current density of 1 A g^{-1}. These results demonstrate the possibility of the integration of flexible solid-state SC with high performance PSCs. Furthermore, an integrated photo-SC device without connecting wire was proposed by Xu et al. A PEDOT:C electrode bridge was used between a mesoscopic carbon-based PSC and the electrode of a SC.[164] The assembled device led to specific energy of 0.78 mW cm^{-2}, power density of 7.4 mW cm^{-2} and maximum overall efficiency up to 4.7%. However, the efficiency dropped exponentially after 1s as the voltage approached that of the solar cell, a trend already observed before.

The integration of PSCs with SC in a single device was also proved by Liu et al. The connection was possible by fabricating a CNT bridge between the PSC and SC parts.[165] SC electrode material was prepared using super-aligned CNTs in combination with polyaniline and H_2SO_4 gel electrolyte. A modified PMMA (polymethyl methacrylate) film was used to avoid water penetration from the electrolyte and degradation of the perovskite layer. After successful integration, the device exhibited a storage efficiency of 70.6%.

Liu et al. successfully integrated PSC and SC in one single device through a shared carbon electrode.[166] The optimal solar cell achieved 7.79% PCE with V_{oc} = 0.96 V, J_{sc} = 15.7 mA $cm^{-2,}$ and FF=0.52. When the integrated device was irradiated at 1 sun, the storage gradually increased and then remained stable after a short time. The voltage plateau during photo-charging was always lower than the V_{oc} of PSC, which depends on the internal resistance of the SC. The maximum overall efficiency was found to be 5.26% with a storage efficiency of 76% for the device with active area of 0.071 cm^2 for a charging voltage of 0.84 V.

High stability and voltage of PSCs were obtained using $CsPbBr_3$ absorber in a meso-porous configuration combined with a nano-carbon layer as hole transporting and shared electrode for

integrated device.[167] The nanocarbon electrode was prepared by doctor-blade coating of conductive carbon ink. Inorganic type absorber in a solar cell configuration exhibited a V_{oc} of 1.22 V much higher than normal organic-inorganic hybrid PSCs, which is beneficial for operation voltage of SC. The SC electrolyte was composed of HCl, TEOS, $TEABF_4$, and concentrated H_3PO_4. The silica-gel electrolyte was carefully deposited on top of the carbon layer and another carbon layer was again deposited on top of the silica-gel electrolyte before annealing at 70 °C for 60 min to obtain all-inorganic solar capacitor. The integrated device afforded overall-efficiency of 5.1% and excellent stability after 1000 charging-discharging cycles. Initially the PCE of carbon-$CsPbBr_3$ solar cells was 6.1% for an active area of 0.1 cm^2.

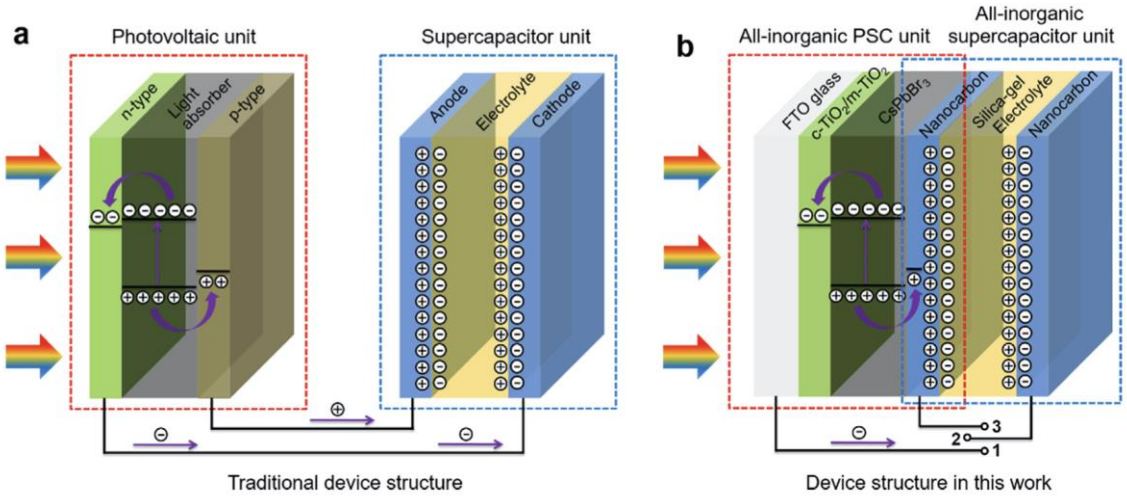

Figure 13. Integrated all-inorganic perovskite solar cell and supercapacitor with (a) separated units and (b) compact configuration using shared carbon electrode. Figure reproduced from Liang et al.[167] with permission from Royal Society of Chemistry.

It should be noted that after optimization, the reported PCE of carbon-based all-inorganic perovskite solar cells reached over 12%. Recently a record-high PCE of 14.84% (active area of 0.09 cm^2) along with excellent storage and operation stability (94%@30 days in air) were

reported.[168] Therefore, the use of such device in a monolithic configuration is extremely interesting for high performance and stable integrated packs.

6. CHALLENGES OF INTEGRATED DEVICES

The photo-supercapacitor technology is in the early stage of development. Researchers have tried various techniques to develop efficient, stable and high-energy PSCs regarding their potential applications in the future. Unfortunately, reported overall efficiencies are considerably low. Many challenges exist and several issues remain to be addressed for the architecture, material capability and the implementation of both devices into a single one through a shared electrode.

The shared electrode is crucial for the photo-supercapacitor as it directly influences the overall performance of the device. Selecting electrodes compatible with both solar cells and supercapacitors is key to reaching good performance. Careful choice of the common electrode may reduce electron recombination and enhance the efficiency, providing that the electrode material is stable towards the interconnected films.[169] Moreover, bridge electrodes with lower internal resistance can reduce the energy dissipation. Flat monolithic shared electrodes, such as silver (Ag) film, limit the surface area and therefore reduce the amount of active material for the supercapacitor, leading to low energy-storage performance.[170] Thus, increasing the surface area of the electrode on the supercapacitor side would be a promising way to achieve higher storage performance.

In the fabrication process, one of the major challenges is the difficulty in encapsulation of both devices with liquid-based electrolytes, which can reduce the performance and the stability due to leakage or material degradation. In perovskite solar cells, liquid electrolyte may damage the perovskite film due to moisture and other chemical reactions. Therefore, proper encapsulation is

required for better stability of the device.[171] Focusing on solid-state and/or quasi solid-state electrolyte for supercapacitors and inorganic perovskite solar cells should be envisaged to enhance the stability of ~~the~~ integrated devices.

In practical application, matching the performance of both solar cell and supercapacitor needs to be considered during the fabrication of photo-supercapacitors. However, in planar structure, a mismatch may exist between solar cell and supercapacitor devices of same physical size leading to lower efficiencies.[172]

Figure 14 displays the areal capacitance versus solar cell efficiency for reported DSC- and PSC/carbon-SCs. The data included are extracted from the available information in the literature and included in the summary displayed in Table S4. In some works, power generation of the solar cell is higher regardless to storage capacity while in some other cases storage capacity is higher regardless to solar power generation. This is due to the physical size of one component limiting the performance of the other component. As shown in Figure 14, PSCs/carbon-SCs yield higher power conversion efficiencies, confirming the potential use of PSCs in future integrated devices.

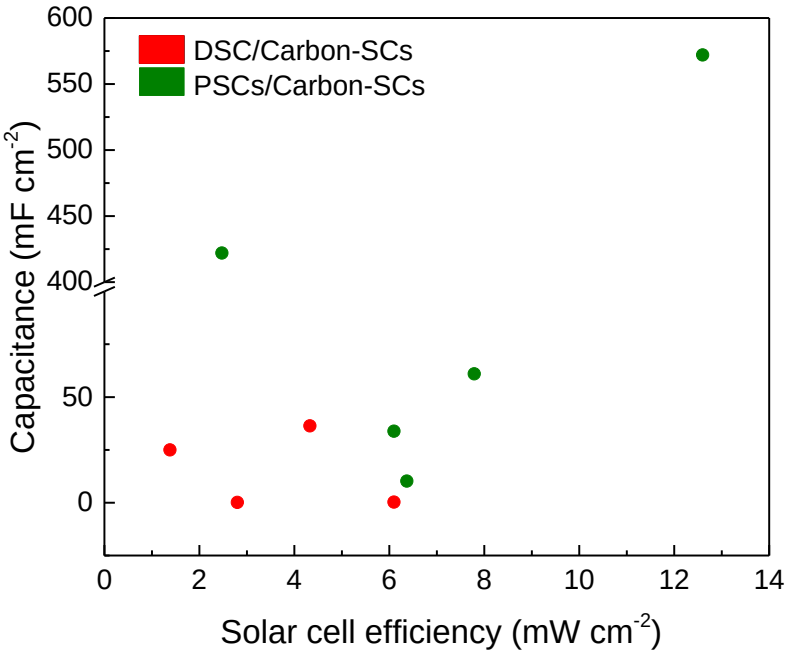

Figure 14. Areal capacitance versus solar cell efficiency for carbon-SCs integrated with DSC or PSCs.

Researchers pay more attention to increase the areal capacitance as much as possible to meet practical needs. Two outperforming carbon based SCs with higher areal capacitances can be noticed. An integrated device with high storage performance of 572 mF cm^{-2} was fabricated by Xu et al. using MWCNTs as electrode material.[16] On the other hand, Liu et al. have developed an integrated device exhibiting the high storage capacitance of 422 mF cm^{-2} using Polyaniline/CNTs composite as electrode material.[165] This excellent storage performance is due to the pseudocapacitive behavior and the higher conductivity of this composite material.

Another possibility is to increase the storage performance and practically useable voltage requirements through widening the working potential of SCs. In general, considering low-power electronics, supercapacitor should be able to deliver at least 60 mW to light up a white LED.[173]

7. SUMMARY AND FUTURE PROSPECTS

Carbon electrodes have been widely used as electrodes for SCs, DSCs, and more recently PSCs. Biomass as a precursor material for AC is preferable since the manufacturing cost and environmental footprint of the devices decreases. By nature, biomass can provide ACs with very high surface area and developed porosity with different pore structures which make them suitable for storage applications. Moreover, due to their high conductivity and favorable band alignment, activated carbons are also well suited to solar cell back-electrodes.

For application as electrode materials in SCs, textural properties (i.e., surface area, pore size and volume) of ACs can be tuned by a proper pyrolysis method or by the nature of the activating agents. Usually, the activation process using strong basic or acidic chemicals such as NaOH, KOH or H_2SO_4 provides a higher surface area compared to the simple pyrolysis method using H_2O or steam as activation agents. As an example, high storage capability of 394 F g^{-1} and specific energy of 23 Wh Kg^{-1} were obtained for aqueous SCs (6M KOH) using AC with a surface area of 2793 m^2 g^{-1}.[5] The later was obtained from willow wood source and KOH as activation agent. The choice of the electrolyte is also an important factor for the fabrication of high-performance SCs with long-term storage stability. Organic electrolytes dominate the market because of their high voltage range. However, due to the volatile nature of organic electrolytes, non-volatile ionic liquids with high potential window are particularly well-suited to be used as electrolytes in SCs. As a result of wide working potentials, ionic liquids can provide high specific energy compared to aqueous and organic electrolytes. The specific capacitance of 224 F g^{-1} and specific energy of 92 Wh kg^{-1} were reported with $EMIMBF_4$ ionic liquid for the porous AC electrodes obtained from pine tree and conventional KOH activation.[64] Due to the numerous parameters affecting the capacitance of ionic liquids SCs, the capacitance value is usually weaker than that measured for aqueous electrolyte

SCs. However, due to their wide potential window the specific energy of ionic liquid SCs is higher than that of aqueous ones which widens the scope of practical applications.

On the other hand, carbon counter-electrodes showed good catalytic properties, long-term chemical and thermal stability in view of replacing expensive Pt counter-electrodes of DSCs. As carbon precursor material, biomass has attracted huge attention for low-cost DSCs and mass production. A PCE of 12.72% was achieved which is, to the best of our knowledge, the highest value reported for carbon nanomaterials as counter-electrodes for DSCs.[42] Here, the porous carbon was obtained by KOH activation of anchovy fish precursor. The porous nature of the material combined with a high electrochemical affinity for the cobalt redox couple yielded such high-performance DSCs, employing SM-315 as sensitizer. Even though the manufacturing cost of devices is decreasing dramatically, several factors limit the practical use of DSCs. This gap can be filled with the new ultrahigh performance solar cells using organic-inorganic hybrid perovskite ($CH_3NH_3PbI_3$, or $MAPbI_3$) as active component. Thanks to their suitable work function, carbon materials can be used as counter-electrode and hole transport material for PSCs. By removing the spiro-OMeTAD and gold layer and adjusting the porous film configuration, a PCE of 15.7% was reported using carbon as counter-electrode and HTM simultaneously.[138] Even if the efficiency of carbon-based PSCs remains low compared to those of standard PSC architectures, the stability was significantly improved to over 14000 hours which makes the device very attractive for industrial applications.

Regarding fully printable carbon-based PSCs, carbon extracted from the biomass is considered by many groups as a key precursor for low-cost devices. The highest PCE of 12.82% was reported for a device prepared with AC from bamboo-chopsticks.[144] Furthermore, by improving the contact between carbon and perovskite layers the efficiency of biomass-based PSCs could be further

enhanced, making them ultra-low-cost solar cell devices. In particular, biomass-carbon PSCs can be efficiently integrated with biomass-carbon SCs for energy conversion-storage devices using a shared carbon electrode. Still, this approach remains overlooked and only few reports on the integration of carbon-based solar cells with storage devices are found in the literature. A maximum overall efficiency of 5.12% was reported for carbon-photo-capacitor using a DSC with 0.36 cm^2 active area.[15] Following the discovery of PSCs, the highest overall efficiency of over 10% was reported for the PSCs/MWCNT/polypyrrole and reduced graphene oxide systems.[16,18] However, these results was reported at the early age of PSCs when the maximum efficiency was still low 12.6% and 13.66% for the active area of 0.06 cm^2 and 1 cm^2, respectively.[16,18] Highly efficient solar cells with large active area and optimized designs would be an option to get high overall efficiency integrated devices. Recent progress on carbon all-inorganic PSCs suggests that these devices are interesting candidates for use in integrated pack.[167,168] Moreover, research efforts in the evaluation of integrated devices are necessary to report reliable and comparable data. Finally, ultra-low-cost biomass materials for energy conversion-and-storage packs are not yet reported, although this would be a significant research interest in the future. New prototypes need to be designed considering specific applications and using stable high-performance PSCs as energy conversion system.

ASSOCIATED CONTENT

Supporting Information

AUTHOR INFORMATION

Corresponding Authors

Thierry Toupance - Université de Bordeaux, Institut des Sciences Moléculaires, UMR 5255 CNRS, 351 Cours de la Libération, F-33405 Talence Cedex, France; Email: thierry.toupance@u-bordeaux.fr; orcid.org/0000-0001-8234-7064

Ludmila Cojocaru - Université de Bordeaux, Institut des Sciences Moléculaires, UMR 5255 CNRS, 351 Cours de la Libération, F-33405 Talence Cedex, France; Email: ludmila.cojocaru@u-bordeaux.fr; orcid.org/0000-0002-3618-4142

Authors

Nilanka M. Keppetipola - Université de Bordeaux, Institut des Sciences Moléculaires, UMR 5255 CNRS, 351 Cours de la Libération, F-33405 Talence Cedex, France

Céline Olivier - Université de Bordeaux, Institut des Sciences Moléculaires, UMR 5255 CNRS, 351 Cours de la Libération, F-33405 Talence Cedex, France; Email: celine.olivier@u-bordeaux.fr; orcid.org/0000-0002-3164-8403

Author Biography

Nilanka M. Keppetipola, is a PhD candidate (Physical chemistry in condense matter) in University of Bordeaux (France). He received his Bachelor's degree in Chemistry and Master's degree in Nanoscience and Nanotechnology from University of Peradeniya, Sri Lanka. His current research focuses on fabrication of integrated device using perovskite solar cells and biomass activated carbon-based supercapacitors for energy conversion and storage devices.

Céline Olivier obtained a PhD in Organic/Organometallic Chemistry from the University of Rennes (France) in 2006. She was appointed Chargé de Recherche CNRS at the Institute of Molecular Sciences of Bordeaux in 2008. Since then, she has been involved in the design and synthesis of molecular photosensitizers for dye-sensitized solar cells and photo-electrochemical cells for solar energy conversion and hydrogen evolution.

Thierry Toupance obtained his PhD in inorganic chemistry from the University Pierre et Marie Curie, Paris (France) and holds a Professorship position at the University of Bordeaux and presently belongs to the "Institute of Molecular Science". His main interests concern the development of functional organic-inorganic hybrid and metal oxide materials for various applications such as photocatalysis, gas sensing and photovoltaic conversion (Dye-sensitized and perovskite solar cells). Currently he deals with the development of nanostructured and/or porous materials for energy storage and conversion applications.

Ludmila Cojocaru, received her PhD from Bordeaux University (France) for her work on the physical chemistry of condensed materials. Subsequently, she was working for two years as post-doc position from the Japan Society of Promotion of Science for Foreign Researchers at the University of Tokyo in the framework of the Japanese French Associate Laboratory for the Next Generation Photovoltaic Cells (LiaNextPV) and

two and half years in a national Japanese project at the University of Tokyo. Her work focused on, materials synthesis, characterization and application in hybrid solar cell technology included liquid (solid)-state dye-sensitized solar cells and perovskite solar cells. Later, she was working at the Institute of Sustainable Technology of the University of Freiburg (Germany), focusing on the evaporation of perovskites for tandem solar cells application, work in collaboration with Fraunhofer Institute for Solar Energy, Germany. Now she is Junior Researcher at Bordeaux University (France) in a Initiative of Excellence “Make Our Planet Great Again”. Her Project is focusing on the fabrication of energy conversion-storage devices. The perovskite solar cells will be integrated with supercapacitors to create energy conversion-storage devices connected through a common electrode based on carbon extracted from biomass.

Author Contributions

The manuscript was written through contributions of all authors. All authors have given approval to the final version of the manuscript.

Funding Sources

This work benefited from the French government assistance, managed funding by the National Research Agency under the "Programme d'Investissements d'Avenir" with the reference "ANR-19-MPGA-0006".

Notes

The authors declare no competing financial interest.

REFERENCES

[1] M. I. A. Abdel Maksoud, R. A. Fahim, A. E. Shalan, M. Abd Elkodous, S. O. Olojede, A. I. Osman, C. Farrell, A. H. Al-Muhtaseb, A. S. Awed, A. H. Ashour and D. W. Rooney, *Environ. Chem. Lett.,* 2021, **19**, 375–739.

[2] J. Gong, K. Sumathy, Q. Qiao and Z. Zhou, *Renew. Sust. Energ. Rev.,* 2017, **68**, 234–246.

[3] A. K. Jena, A. Kulkarni and T. Miyasaka, *Chem. Rev.*, 2019, **119**, 3036–3103.

[4] J. Mi, X. R. Wang, R. J. Fan, W. H. Qu and W. C. Li, *Energy Fuels,* 2012, **26**, 5321–5329.

[5] J. Phiri, J. Dou, T. Vuorinen, P. A. C. Gane and T. C. Maloney, *ACS Omega*, 2019, **4**, 18108–18117.

[6] C. Y. Bon, L. Mohammed, S. Kim, M. Manasi, P. Isheunesu, K. S. Lee and J. M. Ko, *J. Ind. Eng. Chem.*, 2018, **68**, 173–179.

[7] E. Frackowiak, *Phys. Chem. Chem. Phys.*, 2007, **9**, 1774-1785.

[8] H. Lu and X. S. Zhao, *Sustain. Energy Fuels,* 2017, **1**, 1265-1281.

[9] Y. Wang, Q. Qu, S. Gao, G. Tang, K. Liu, S. He and C. Huang, *Carbon,* 2019, **155**, 706-726.

[10] M. Hadadian, J-H. Smatt, J-P. Correra-Baena, *Energy Environ. Sci*., 2020, **13**, 1377-1407.

[11] F. Meng, A. Liu, L. Gao, J. Cao, Y. Yan, N. Wang, M. Fan, G. Wei, T. Ma, *J. Mater. Chem. A*, 2019, **7**, 8690-8699.

[12] Y. Qiang, L. Zhang, S. Shao and J. Li, *Int. J. Energy Res.*, 2021, **45**, 6426-6435.

[13] A. Gurung, K. Chen, R. Khan, S. S. Abdulkarim, G. Varnekar, R. Pathak, R. Naderi and Q. Qiao, *Adv. Energy Mater.*, 2017, **7**, 1602105.

[14] H. Zhang, Y. Lu, W. Han, J. Zhu, Y. Zhang and W. Huang, *Chem. Eng. J.*, 2020, **393**, 124766.

[15] Z. Yang, L. Li, Y. Luo, R. He, L. Qiu, H. Lin and H. Peng, *J. Mater. Chem. A*, 2013, **1**, 954–958.

[16] X. Xu, S. Li, H. Zhang, Y. Shen, S. M. Zakeeruddin, M. Graetzel, Y. B. Cheng and M. Wang, *ACS Nano*, 2015, **9**, 1782–1787.

[17] A. K. Mohammed, V. Vijayakumar, A. Halder, M. Ghosh, M. Addicoat, U. Bansode, S. Kurungot and R. Banerjee, *ACS Appl. Mater. Interfaces*, 2019, **11**, 30828-30837.

[18] J. Kim, S. M. Lee, Y. H. Hwang, S. Lee, B. Park, J. H. Jang and K. Lee, *J. Mater. Chem. A*, 2017, **5**, 1906-1912.

[19] J. H. Lee and S. J. Park, *Carbon N. Y.*, 2020, **163**, 1-18.

[20] W. Zhang, S. Zhu, R. Luque, S. Han, L. Hu and G. Xu, *Chem. Soc. Rev.*, 2016, **45**, 715-752.

[21] M. Danish and T. Ahmad, *Renew. Sustain. Energy Rev.*, 2018, **87**, 1–21.

[22] Y. Zou and B. X. Han*, Energy Fuels,* 2001, **15**, 1383–1386.

[23] H. Gu, R. Bergman, N. Anderson and S. Alanya-Rosenbaum, *Wood Fiber Sci.*, 2018, **50**, 229–243.

[24] O. Ioannidou and A. Zabaniotou, *Renew. Sustain. Energy Rev.,* 2007, **11**, 1966–2005.

[25] J. Bedia, M. Peñas-Garzón, A. Gómez-Avilés, J. Rodriguez and C. Belver, *C.*, 2018, **4**, 63.

[26] J. Pallarés, A. González-Cencerrado and I. Arauzo, *Biomass and Bioenergy*, 2018, **115**, 64–73.

[27] D. Jimenez-Cordero, F. Heras, N. Alonso-Morales, M. A. Gilarranz and J. J. Rodriguez, *Biomass and Bioenergy*, 2013, **54**, 123–132.

[28] L. Leng, Q. Xiong, L. Yang, H. Li, Y. Zhou, W. Zhang, S. Jiang, H. Li and H. Huang, *Sci. Total Environ.*, 2021, **763**, 144204.

[29] F. Salvador, M. J. Sánchez-Montero and C. Izquierdo, *J. Phys. Chem. C*, 2007, **111**, 14011–14020.

[30] M. A. Yahya, Z. Al-Qodah and C. W. Z. Ngah, *Renew. Sustain. Ener. Rev.*, 2015, **46**, 218–235.

[31] Y. Gao, Q. Yue, B. Gao and A. Li, *Sci. Total Environ.*, 2020, **746**, 141094.

[32] K. Le Van and T. T. Luong Thi, *Prog. Nat. Sci. Mater. Int.*, 2014, **24**, 191–198.

[33] E. Cetin, R. Gupta and B. Moghtaderi, *Fuel,* 2005, **84**, 1328–1334.

[34] P. Fu, S. Hu, J. Xiang, L. Sun, P. Li, J. Zhang and C. Zheng, *Energy Fuels,* 2009, **23**, 4605–4611.

[35] Y. Sun, H. Li, G. Li, B. Gao, Q. Yue and X. Li, *Bioresour. Technol.*, 2016, **217**, 239–244.

[36] A. Kumar and H. M. Jena, *Process Saf. Environ. Prot.*, 2017, **109**, 63–71.

[37] A. Gundogdu, C. Duran, H. B. Senturk, M. Soylak, M. Imamoglu and Y. Onal, *J. Anal. Appl. Pyrolysis*, 2013, **104**, 249–259.

[38] G. Özsin, M. Kılıç, E. Apaydın-Varol and A. E. Pütün, *Appl. Water Sci.,* 2019, **9**, 56.

[39] M. Iwanow, T. Gärtner, V. Sieber and B. König, *Beilstein J. Org. Chem.*, 2020, **16**, 1188-1202.

[40] C. Hu and L. Dai, *Adv. Mater.*, 2019, **31**, 1804672.

[41] M. Chen, R.-H. Zha, Z.-Y. Yuan, Q.-S. Jing, Z.-Y. Huang, X.-K. Yang, S.-M. Yang, X.-H. Zhao, D.-L. Xu and G.-D. Zou, *Chem. Eng. J.*, 2017, **313**, 791–800.

[42] C. K. Kim, I. T. Choi, S. H. Kang and H. K. Kim, *RSC Adv.*, 2017, **7**, 35565–35574.

[43] D.-Y. Shin, K.-W. Sung and H.-J. Ahn, *Appl. Surf. Sci.*, 2019, **478**, 499–504.

[44] A. Gopalakrishnan and S. Badhulika, *J. Power Sources*, 2020, **480**, 228830.

[45] J. Vatamanu, O. Borodin, M. Olguin, G. Yushin and D. Bedrov, *J. Mater. Chem. A*, 2017, **5**, 21049–21076.

[46] S. Banerjee, B. De, P. Sinha, J. Cherusseri and K. K. Kar, *Springer Ser Mater. Sci.*, 2020, **300**, 341–350.

[47] P. Simon and Y. Gogotsi, *Nat. Mater.*, 2008, **7**, 845-854.

[48] J. Zhao and A. F. Burke, *J. Energy Chem.*, 2021, **59**, 276-291.

[49] B. K. Kim, S. Sy, A. Yu and J. Zhang, *Handbook of Clean Energy Systems*, 2015, 1–25.

[50] H. Yang, S. Ye, J. Zhou and T. Liang, *Front. Chem.*, 2019, **7**, 1-17.

[51] C. Zequine, C. K. Ranaweera, Z. Wang, S. Singh, P. Tripathi, O. N. Srivastava, B. K. Gupta, K. Ramasamy, P. K. Kahol, P. R. Dvornic and R. K. Gupta, *Sci. Rep.*, 2016, **6**, 31704.

[52] E. Frackowiak and F. Béguin, *Carbon N. Y.*, 2001, **39**, 937–950.

[53] S. Ghosh, R. Santhosh, S. Jeniffer, V. Raghavan, G. Jacob, K. Nanaji, P. Kollu, S. K. Jeong and A. N. Grace, *Sci. Rep.*, 2019, **9**, 16315.

[54] Z. Gao, Y. Zhang, N. Song and X. Li, *Mater. Res. Lett.*, 2017, **5**, 69-88.

[55] M. Wahid, G. Parte, D. Phase and S. Ogale, *J. Mater. Chem. A*, 2015, **3**, 1208–1215.

[56] H. Yang, S. Kannappan, A. S. Pandian, J. H. Jang, Y. S. Lee and W. Lu, *Nanotechnology*, 2017, **28**, 445101.

[57] A. B. Fuertes, F. Pico and J. M. Rojo, *J. Power Sources*, 2004, **133**, 329–336.

[58] C. Largeot, C. Portet, J. Chmiola, P. L. Taberna, Y. Gogotsi and P. Simon, *J. Am. Chem. Soc.*, 2008, **130**, 2730–2731.

[59] J. Chmiola, G. Yushin, Y. Gogotsi, C. Portet, P. Simon and P. L. Taberna, *Sci.,* 2006, **313**, 1760–1763.

[60] S. Qu, J. Wan, C. Dai, T. Jin and F. Ma, *J. Alloys Compd.*, 2018, **751**, 107–116.

[61] S. Yang, S. Wang, X. Liu and L. Li, *Carbon N. Y.*, 2019, **147**, 540–549.

[62] W. Sun, S. M. Lipka, C. Swartz, D. Williams and F. Yang, *Carbon N. Y.*, 2016, **103**, 181–192.

[63] M. Olivares-Marín, J. A. Fernández, M. J. Lázaro, C. Fernández-González, A. Macías-García, V. Gómez-Serrano, F. Stoeckli and T. A. Centeno, *Mater. Chem. Phys.*, 2009, **114**, 323–327.

[64] X. Wang, Y. Li, F. Lou, M. E. Melandsø Buan, E. Sheridan and D. Chen, *RSC Adv.*, 2017, **7**, 23859–23865.

[65] M. Karnan, K. Subramani, N. Sudhan, N. Ilayaraja and M. Sathish, *ACS Appl. Mater. Interfaces*, 2016, **8**, 35191–35202.

[66] N. M. Keppetipola, M. Dissanayake, P. Dissanayake, B. Karunarathne, M. A. Dourges, D. Talaga, L. Servant, C. Olivier, T. Toupance, S. Uchida, K. Tennakone, G. R. A. Kumara and L. Cojocaru, *RSC Adv.*, 2021, **11**, 2854–2865.

[67] E. Y. L. Teo, L. Muniandy, E. P. Ng, F. Adam, A. R. Mohamed, R. Jose and K. F. Chong, *Electrochim. Acta*, 2016, **192**, 110–119.

[68] T. E. Rufford, D. Hulicova-Jurcakova, Z. Zhu and G. Q. Lu, *J. Phys. Chem. C*, 2009, **113**, 19335–19343.

[69] A. Elmouwahidi, Z. Zapata-Benabithe, F. Carrasco-Marín and C. Moreno-Castilla, *Bioresour. Technol.*, 2012, **111**, 185–190.

[70] M. Z. Iqbal, S. Zakar and S. S. Haider, *J. Electroanal. Chem.*, 2020, **828**, 113793.

[71] B. Pal, S. Yang, S. Ramesh, V. Thangadurai and R. Jose, *Nanoscale Adv.*, 2019, **1**, 3807–3835.

[72] S. Pan, M. Yao, J. Zhang, B. Li, C. Xing, X. Song, P. Su and H. Zhang, *Front. Chem.*, 2020, **8**, 261.

[73] L. Yu and G. Z. Chen, *Front. Chem.*, 2019, **7**, 272.

[74] B. O'Regan and M. Grätzel, *Nature*, 1991, **353**, 737–740.

[75] A. Kojima, K. Teshima, Y. Shirai and T. Miyasaka, *J. Am. Chem. Soc.*, 2009, **131**, 6050–6051.

[76] H. Gerischer, M. E. Michel-Beyerle, F. Rebentrost and H. Tributsch, *Electrochim. Acta*, 1968, **13**, 1509–1515.

[77] K. Kakiage, Y. Aoyama, T. Yano, K. Oya, J. Fujisawa and M. Hanaya, *Chem. Commun.*, 2015, **51**, 15894–15897.

[78] A. Yella, H. W. Lee, H. N. Tsao, C. Yi, A. K. Chandiran, M. K. Nazeeruddin, E. W. G. Diau, C. Y. Yeh, S. M. Zakeeruddin and M. Grätzel, *Sci.,* 2011, **334**, 629–634.

[79] M. Green, E. Dunlop, J. Hohl-Ebinger, M. Yoshita, N. Kopidakis and X. Hao, *Prog. Photovoltaics Res. Appl.*, 2021, **29**, 3–15.

[80] U. Bach, D. Lupo, P. Comte, J. E. Moser, F. Weissörtel, J. Salbeck, H. Spreitzer and M. Grätzel, *Nature*, 1998, **395**, 583–585.

[81] J. Burschka, A. Dualeh, F. Kessler, E. Baranoff, N. L. Cevey-Ha, C. Yi, M. K. Nazeeruddin and M. Grätzel, *J. Am. Chem. Soc.*, 2011, **133**, 18042–18045.

[82] H.-S. Kim, C.-R. Lee, J.-H. Im, K.-B. Lee, T. Moehl, A. Marchioro, S.-J. Moon, R. Humphry-Baker, J.-H. Yum, J. E. Moser, M. Grätzel and N.-G. Park, *Sci. Rep.*, 2012, **2**, 591.

[83] W. E. I. Sha, X. Ren, L. Chen and W. C. H. Choy, *Appl. Phys. Lett.*, 2015, **106**, 221104.

[84] M. I. Hossain, W. Qarony, S. Ma, L. Zeng, D. Knipp and Y. H. Tsang, *Nano-Micro Lett.*, 2019, **11**, 58.

[85] T. N. Murakami, S. Ito, Q. Wang, M. K. Nazeeruddin, T. Bessho, I. Cesar, P. Liska, R. Humphry-Baker, P. Comte, P. Péchy and M. Grätzel, *J. Electrochem. Soc.*, 2006, **153**, A2255.

[86] C.-S. Wu, T.-W. Chang, H. Teng and Y.-L. Lee, *Ener.*, 2016, **115**, 513–518.

[87] C.-T. Li, C.-T. Lee, S.-R. Li, C.-P. Lee, I.-T. Chiu, R. Vittal, N.-L. Wu, S.-S. Sun and K.-C. Ho, *J. Power Sources*, 2016, **302**, 155–163.

[88] A. S. A. Ahmed, W. Xiang, A. Gu, X. Hu, I. A. Saana and X. Zhao, *New J. Chem.*, 2018, **42**, 11715–11723.

[89] I.-P. Liu, Y.-C. Hou, C.-W. Li and Y.-L. Lee, *J. Mater. Chem. A*, 2017, **5**, 240–249.

[90] Y. Xu, H. Bai, G. Lu, C. Li and G. Shi, *J. Am. Chem. Soc.*, 2008, **130**, 5856–5857.

[91] W. Wei, K. Sun and Y. H. Hu, *J. Mater. Chem. A*, 2016, **4**, 12054–12057.

[92] C.-A. Tseng, C.-P. Lee, Y.-J. Huang, H.-W. Pang, K.-C. Ho and Y.-T. Chen, *Mater. Today Ener.*, 2018, **8**, 15–21.

[93] X. Meng, C. Yu, X. Song, Z. Liu, B. Lu, C. Hao and J. Qiu, *J. Mater. Chem. A*, 2017, **5**, 2280–2287.

[94] F. Gong, H. Wang and Z. S. Wang, *Phys. Chem. Chem. Phys.*, 2011, **13**, 17676–17682.

[95] D. Wu, C. Zhu, Y. Shi, H. Jing, J. Hu, X. Song, D. Si, S. Liang and C. Hao, *ACS Sustain. Chem. Eng.*, 2019, **7**, 1137–1145.

[96] K. Suzuki, M. Yamaguchi, M. Kumagai and S. Yanagida, *Chem. Lett.*, 2003, **32**, 28–29.

[97] W. J. Lee, E. Ramasamy, D. Y. Lee and J. S. Song, *ACS Appl. Mater. Interfaces*, 2009, **1**, 1145–1149.

[98] A. Monreal-Bernal, J. J. Vilatela and R. D. Costa, *Carbon N. Y.*, 2019, **141**, 488–496.

[99] M. R. Al-bahrani, W. Ahmad, S.-S. Ruan, Z. Yang, Z. Cheng and Y. Gao, *RSC Adv.*, 2015, **5**, 95551–95557.

[100] A. A. Arbab, K. C. Sun, I. A. Sahito, M. B. Qadir, Y. S. Choi and S. H. Jeong, *ACS Appl. Mater. Interfaces*, 2016, **8**, 7471–7482.

[101] F. Yu, Y. Shi, W. Yao, S. Han and J. Ma, *J. Power Sources*, 2019, **412**, 366–373.

[102] X. Wang, Y. Xie, Y. Jiao, K. Pan, B. Bateer, J. Wu and H. Fu, *J. Mater. Chem. A*, 2019, **7**, 10405–10411.

[103] https://www.nrel.gov/pv/assets/pdfs/best-research-cell-efficiencies.20200104.pdf, (updated 01/04/2021)

[104] H. Jing, Y. Shi, D. Wu, S. Liang, X. Song, Y. An and C. Hao, *Electrochim. Acta*, 2018, **281**, 646–653.

[105] H. Jing, D. Wu, S. Liang, X. Song, Y. An, C. Hao and Y. Shi, *J. Ener. Chem.*, 2019, 89–94.

[106] K. D. M. S. P. K. Kumarasinghe, G. R. A. Kumara, R. M. G. Rajapakse, D. N. Liyanage and K. Tennakone, *Org. Electron.*, 2019, **71**, 93–97.

[107] C. Xiang, T. Lv, C. A. Okonkwo, M. Zhang, L. Jia and W. Xia, *J. Electrochem. Soc.*, 2017, **164**, H203–H210.

[108] G. Nagaraju, J. H. Lim, S. M. Cha and J. S. Yu, *J. Alloys Compd.*, 2017, **693**, 1297–1304.

[109] D. Y. Chung, Y. J. Son, J. M. Yoo, J. S. Kang, C. Y. Ahn, S. Park and Y. E. Sung, *ACS Appl. Mater. Interfaces*, 2017, **9**, 41303–41313.

[110] P. Ma, W. Lu, X. Yan, W. Li, L. Li, Y. Fang, X. Yin, Z. Liu and Y. Lin, *RSC Adv.*, 2018, **8**, 18427–18433.

[111] S. M. Cha, G. Nagaraju, S. C. Sekhar, L. K. Bharat and J. S. Yu, *J. Colloid Interface Sci.*, 2018, **513**, 843–851.

[112] Y. Zhang, S. Yun, C. Wang, Z. Wang, F. Han and Y. Si, *J. Power Sources*, 2019, **423**, 339–348.

[113] C. L. Wang, J. Y. Liao, S. H. Chung and A. Manthiram, *Adv. Ener. Mater.*, 2015, **5**, 1401524.

[114] J. P. Correa-Baena, M. Saliba, T. Buonassisi, M. Grätzel, A. Abate, W. Tress and A. Hagfeldt, *Sci.,* 2017, **358**, 739–744.

[115] S. Svanström, T. J. Jacobsson, G. Boschloo, E. M. J. Johansson, H. Rensmo and U. B. Cappel, *ACS Appl. Mater. Interfaces*, 2020, **12**, 7212–7221.

[116] D. Bogachuk, S. Zouhair, K. Wojciechowski, B. Yang, V. Babu, L. Wagner, B. Xu, J. Lim, S. Mastroianni, H. Pettersson, A. Hagfeldt and A. Hinsch, *Energy Environ. Sci.*, 2020, **13**, 3880–3916.

[117] F. Zhang, X. Yang, H. Wang, M. Cheng, J. Zhao and L. Sun, *ACS Appl. Mater. Interfaces*, 2014, **6**, 16140–16146.

[118] H. N. Chen, Z. H. Wei, H. X. He, X. L. Zheng, K. S. Wong and S. H. Yang, *Adv. Energy Mater.*, 2016, **6**, 1502087.

[119] X. Chang, W. Li, H. Chen, L. Zhu, H. Liu, H. Geng, S. Xiang, J. Liu, X. Zheng, Y. Yang and S. Yang, *ACS Appl. Mater. Interfaces*, 2016, **8**, 30184–30192.

[120] H. Chen, X. Zheng, Q. Li, Y. Yang, S. Xiao, C. Hu, Y. Bai, T. Zhang, K. S. Wong and S. Yang, *J. Mater. Chem. A*, 2016, **4**, 12897–12912.

[121] J. Zhang, C. Wang, H. Fu, L. Gong, H. He, Z. Fang, C. Zhou, J. Chen, Z. Chao and J. Fan, *J. Alloys Compd.*, 2020, **862**, 158454.

[122] Y. Yang, J. Xiao, H. Wei, L. Zhu, D. Li, Y. Luo, H. Wu and Q. Meng, *RSC Adv.*, 2014, **4**, 52825–52830.

[123] F. Zhang, X. Yang, M. Cheng, W. Wang and L. Sun, *Nano Energy*, 2016, **20**, 108–116.

[124] X. Jiang, Z. Yu, H.-B. Li, Y. Zhao, J. Qu, J. Lai, W. Ma, D. Wang, X. Yang and L. Sun, *J. Mater. Chem. A*, 2017, **5**, 17862–17866.

[125] X. Liu, Z. Liu, B. Sun, X. Tan, H. Ye, Y. Tu, T. Shi, Z. Tang and G. Liao, *Nano Energy*, 2018, **50**, 201–211.

[126] T. Liu, L. Liu, M. Hu, Y. Yang, L. Zhang, A. Mei and H. Han, *J. Power Sources*, 2015, **293**, 533–538.

[127] K. Cao, Z. Zuo, J. Cui, Y. Shen, T. Moehl, S. M. Zakeeruddin, M. Grätzel and M. Wang, *Nano Energy*, 2015, **17**, 171–179.

[128] A. Mei, X. Li, L. Liu, Z. Ku, T. Liu, Y. Rong, M. Xu, M. Hu, J. Chen, Y. Yang, M. Grätzel and H. Han, *Sci.*, 2014, **345**, 295–298.

[129] X. Jiang, Y. Xiong, Z. Zhang, Y. Rong, A. Mei, C. Tian, J. Zhang, Y. Zhang, Y. Jin, H. Han and Q. Liu, *Electrochim. Acta*, 2018, **263**, 134–139.

[130] Z. Li, S. A. Kulkarni, P. P. Boix, E. Shi, A. Cao, K. Fu, S. K. Batabyal, J. Zhang, Q. Xiong, L. H. Wong, N. Mathews and S. G. Mhaisalkar, *ACS Nano*, 2014, **8**, 6797–6804.

[131] Z. Wei, H. Chen, K. Yan, X. Zheng and S. Yang, *J. Mater. Chem. A*, 2015, **3**, 24226–24231.

[132] Q. Luo, H. Ma, Y. Zhang, X. Yin, Z. Yao, N. Wang, J. Li, S. Fan, K. Jiang and H. Lin, *J. Mater. Chem. A*, 2016, **4**, 5569–5577.

[133] Y. Wang, H. Zhao, Y. Mei, H. Liu, S. Wang and X. Li, *ACS Appl. Mater. Interfaces*, 2019, **11**, 916–923.

[134] Y. Zhu, S. Jia, J. Zheng, Y. Lin, Y. Wu and J. Wang, *J. Mater. Chem. C*, 2018, **6**, 3097–3103.

[135] W. Wei, B. Hu, F. Jin, Z. Jing, Y. Li, A. A. García Blanco, D. J. Stacchiola and Y. H. Hu, *J. Mater. Chem. A*, 2017, **5**, 7749–7752.

[136] K. Yan, Z. Wei, J. Li, H. Chen, Y. Yi, X. Zheng, X. Long, Z. Wang, J. Wang, J. Xu and S. Yang, *Small*, 2015, **11**, 2269–2274.

[137] M. Jeong, I. W. Choi, E. M. Go, Y. Cho, M. Kim, B. Lee, S. Jeong, Y. Jo, H. W. Choi, J. Lee, J. H. Bae, S. K. Kwak, D. S. Kim and C. Yang, *Sci.*, 2020, **369**, 1615-1620.

[138] C. Tian, A. Mei, S. Zhang, H. Tian, S. Liu, F. Qin, Y. Xiong, Y. Rong, Y. Hu, Y. Zhou, S. Xie and H. Han, *Nano Energy*, 2018, **53**, 160–167.

[139] S. Liu, S. Li, J. Wu, Q. Wang, Y. Ming, D. Zhang, Y. Sheng, Y. Hu, Y. Rong, A. Mei and H. Han, *J. Phys. Chem. Lett.*, 2019, **10**, 6865–6872.

[140] S. S. Mali, H. Kim, J. V. Patil and C. K. Hong, *ACS Appl. Mater. Interfaces*, 2018, **10**, 31280–31290.

[141] Rembianov, L. Kevin, J. Sulistianto and N. R. Poespawati, in *2019 11th International Conference on Information Technology and Electrical Engineering, ICITEE 2019*, 2019.

[142] S. Pitchaiya, N. Eswaramoorthy, M. Natarajan, A. Santhanam, V. Asokan, V. Madurai Ramakrishnan, B. Rangasamy, S. Sundaram, P. Ravirajan and D. Velauthapillai, *Sci. Rep.*, 2020, **10**, 6835.

[143] H. Liu, Y. Xie, P. Wei, W. Wang, H. Chen, C. Geng and Y. Qiang, *J. Alloys Compd.* 2020, **842**, 155851.

[144] L. Gao, Y. Zhou, F. Meng, Y. Li, A. Liu, Y. Li, C. Zhang, M. Fan, G. Wei and T. Ma, *Carbon N. Y.*, 2020, **162**, 267–272.

[145] B. P. Lechene, R. Clerc and A. C. Arias, *Sol. Energy Mater. Sol. Cells*, 2017, **172**, 202–212.

[146] L. C. Kin, Z. Liu, O. Astakhov, S. N. Agbo, H. Tempel, S. Yu, H. Kungl, R. A. Eichel, U. Rau, T. Kirchartz and T. Merdzhanova, *ACS Appl. Energy Mater.*, 2020, **3**, 431–439.

[147] A. S. Westover, K. Share, R. Carter, A. P. Cohn, L. Oakes and C. L. Pint, *Appl. Phys. Lett.* 2014, **104**, 213905.

[148] S. S.-Y. Juang, P.-Y. Lin, Y.-C. Lin, Y.-S. Chen, P.-S. Shen, Y.-L. Guo, Y.-C. Wu and P. Chen, *Front. Chem*., 2019, **7**, 1-9.

[149] L. Cojocaru, S. Uchida, K. Tamaki, P. V. V. Jayaweera, S. Kaneko, J. Nakazaki, T. Kubo and H. Segawa, *Sci. Rep.* 2017, **7**, 11790.

[150] Miyasaka and T. N. Murakami, *Appl. Phys. Lett.*, 2004, **85**, 3932–3934.

[151] H. Nagai and H. Segawa, *Chem. Commun.*, 2004, **4**, 974–975.T.

[152] T. N. Murakami, N. Kawashima and T. Miyasaka, *Chem. Commun.*, 2005, 3346–3348.

[153] N. Bagheri, A. Aghaei, M. Y. Ghotbi, E. Marzbanrad, N. Vlachopoulos, L. Häggman, M. Wang, G. Boschloo, A. Hagfeldt, M. Skunik-Nuckowska and P. J. Kulesza, *Electrochim. Acta*, 2014, **143**, 390–397.

[154] J. Bae, Y. J. Park, M. Lee, S. N. Cha, Y. J. Choi, C. S. Lee, J. M. Kim and Z. L. Wang, *Adv. Mater.*, 2011, **23**, 3446–3449.

[155] T. Chen, L. Qiu, Z. Yang, Z. Cai, J. Ren, H. Li, H. Lin, X. Sun and H. Peng, *Angew. Chemie Int. Ed.*, 2012, **51**, 11977–11980.

[156] X. Chen, H. Sun, Z. Yang, G. Guan, Z. Zhang, L. Qiu and H. Peng, *J. Mater. Chem. A*, 2014, **2**, 1897–1902.

[157] Z. Yang, J. Deng, H. Sun, J. Ren, S. Pan and H. Peng, *Adv. Mater.*, 2014, **26**, 7038–7042.

[158] A. Scalia, F. Bella, A. Lamberti, S. Bianco, C. Gerbaldi, E. Tresso and C. F. Pirri, *J. Power Sources*, 2017, **359**, 311–321.

[159] A. Scalia, F. Bella, A. Lamberti, C. Gerbaldi and E. Tresso, *Energy*, 2019, **166**, 789–795.

[160] A. Scalia, A. Varzi, A. Lamberti, T. Jacob and S. Passerini, *Front. Chem.*, 2018, **6**, 443.

[161] P. Dong, M. T. F. Rodrigues, J. Zhang, R. S. Borges, K. Kalaga, A. L. M. Reddy, G. G. Silva, P. M. Ajayan and J. Lou, *Nano Energy*, 2017, **42**, 181–186.

[162] X. Hou, Y. Wang, H. K. H. Lee, R. Datt, N. Uslar Miano, D. Yan, M. Li, F. Zhu, B. Hou, W. C. Tsoi and Z. Li, *J. Mater. Chem. A*, 2020, **8**, 21503–21525.

[163] P. Du, X. Hu, C. Yi, H. C. Liu, P. Liu, H. L. Zhang and X. Gong, *Adv. Funct. Mater.*, 2015, **25**, 2420–2427.

[164] J. Xu, Z. Ku, Y. Zhang, D. Chao and H. J. Fan, *Adv. Mater. Technol.*, 2016, **1**, 1600074.

[165] R. Liu, C. Liu and S. Fan, *J. Mater. Chem. A*, 2017, **5**, 23078–23084.

[166] Z. Liu, Y. Zhong, B. Sun, X. Liu, J. Han, T. Shi, Z. Tang and G. Liao, *ACS Appl. Mater. Interfaces*, 2017, **9**, 22361–22368.

[167] J. Liang, G. Zhu, C. Wang, P. Zhao, Y. Wang, Y. Hu, L. Ma, Z. Tie, J. Liu and Z. Jin, *Nano Energy*, 2018, **52**, 239–245.

[168] W. Zhu, W. Chai, D. Chen, J. Ma, D. Chen, H. Xi, J. Zhang, C. Zhang and Y. Hao, *ACS Energy Lett.*, 2021, **6**, 1500–1510.

[169] K. Namsheer and C. S. Rout, *J. Mater. Chem. A*, 2021, **9**, 8248–8278.

[170] J. Shin, V. H. Tran, D. C. Tien Nguyen, S. K. Kim and S. H. Lee, *Org. Electron.*, 2021, **89**, 106050.

[171] Y. Sun and X. Yan, *Sol. RRL*, 2017, **1**, 1700002.

[172] D. Schmidt, M. D. Hager and U. S. Schubert, *Adv. Energy Mater.*, 2016, **6**, 1500369.

[173] V. Vega-Garita, L. Ramirez-Elizondo, N. Narayan and P. Bauer, *Prog. Photovoltaics Res. Appl.*, 2019, **27**, 346–370.